Mathematical Results for Slipping Flows Past a Cylinder or a Sphere Embedded in a Porous Medium

by

NADA ALSHEHRI
Summer 2015

A Thesis Submitted
in Partial Fulfillment
of the Requirements for Degree of

MASTER OF SCIENCE

The Graduate Mathematics Program
Applied and Computational Mathematics Option
Department of Mathematics and Statistics
Texas A&M University - Corpus Christi

APPROVED: _____ Date: _____
Dr. Devanayagam Palaniappan, Chair

_____
Dr. Diane Denny, Member

_____
Dr. Dugan Um, Member

_____
Dr. George Tintera, Chair
Department of Mathematics and Statistics

_____
Dr. Frank Pezold, Dean
College of Science and Engineering

Style: Proceedings of the American Mathematical Society

Contents

1 Introduction **1**

2 Darcy, Brinkman models, and Navier-slip boundary conditions **5**
2.1 Darcy model 5
2.2 Brinkman model 6
2.3 Navier-slip boundary conditions 7

3 Brinkman flows past a cylinder (Two-dimensional flows) **9**
3.1 Uniform flow past a cylinder 12
3.1.1 Streamline patterns 14
3.1.2 Tangential velocity and shear stress 17
3.1.3 Pressure and vorticity for uniform flow past a cylinder 19
3.2 Shear flow past a cylinder 21
3.2.1 Streamline patterns 22
3.2.2 Tangential velocity and shear stress 24
3.2.3 Pressure and vorticity for shear flow past a cylinder . . 26

4 Brinkman flows past a sphere (Three-dimensional flows) **28**
4.1 Uniform flow past a sphere 30
4.1.1 Streamline patterns 32
4.1.2 Tangential velocity and shear stress 33
4.1.3 Pressure and vorticity for uniform flow past a sphere . 36
4.2 Shear flow past a sphere 38
4.2.1 Streamline Patterns 39
4.2.2 Tangential velocity and shear stress 41
4.2.3 Pressure and vorticity for shear flow past a sphere . . . 43

5 Force for the uniform flow past a cylinder/sphere **45**

6 Conclusion **48**

Appendix A: *Derivation of the general solution for two-dimensional flows* **52**

Appendix B: *Derivation of the general solution for three-dimensional flows* **56**

Appendix C: *Some properties of the modified Bessel functions of second kind* **60**

List of Figures

1 A sample physical model for flow past a solid inclusion in a porous medium. 2
2 Description of the two-dimensional coordinate system. A steady incompressible flow with the velocity $\mathbf{u}_0$ is due to a basic flow field. 9
3 Streamline patterns for uniform flow past a cylinder with radius $a = 1$ and $\delta = .001$: (a) $\xi = 0$ (b) $\xi = .01$ (c) $\xi = .5$ (d) $\xi = 3$. 14
4 Streamline patters for uniform flow past a cylinder with radius $a = 1$ and $\delta = 5$: (a) $\xi = 0$ (b) $\xi = .01$ (c) $\xi = .5$ (d) $\xi = 3$. . . 15
5 Streamline patterns for uniform flow past a cylinder with radius $a = 1$ and $\xi = .1$: (a) $\delta = .01$ (b) $\delta = .5$ (c) $\delta = 5$ (d) $\delta = 100$. 15
6 Streamline patterns for uniform flow past a cylinder with radius $a = 1$ and $\xi = .7$: (a) $\delta = .01$ (b) $\delta = .5$ (c) $\delta = 5$ (d) $\delta = 100$. 16
7 Variation of u_θ with r: (a) $\delta = 1$ (b) $\delta = 5$ (c) $\xi = 0$ (d) $\xi = 0.5$. 17
8 Variation of $\tau_{r\theta}$ with θ: (a) $\delta = 1$ (b) $\delta = 5$, (c) $\xi = 0$ (d) $\xi = 0.5$. 18
9 Variation of $p(r)$ with r where $\theta = 0^o$: (a)$\delta = 0.1$ (b)$\delta = 1$. . . 20
10 Variation of ω with r where $\theta = \frac{\pi}{2}$: (a)$\xi = 0.01$ (b)$\xi = 0.5$. . . 21
11 Streamline patterns for shear flow past a circular cylinder with a radius $a = 1$, $\delta = .001$ and $\delta = 5$: (a) $\xi = 0$ (b) $\xi = .5$ (c) $\xi = 1$ 23
12 Streamline patterns for shear flow past a circular cylinder with a radius $a = 1$, $\xi = .1$ and $\xi = 0.5$ (a) $\delta = .1$ (b) $\delta = .5$ (c) $\delta = 1$. 23
13 Variation of u_θ with r: (a) $\delta = 1$ (b) $\delta = 5$ (c) $\xi = 0$ (d) $\xi = 0.5$. 25
14 Variation of $\tau_{r\theta}$ with θ: (a) $\delta = 1$ (b) $\xi = 0$. 25
15 Variation of $p(r)$ with r while $\theta = 0^o$: (a) $\delta = .1$ (b) $\delta = 1$. . . 27
16 Variation of ω with r while $\theta = \frac{\pi}{4}$: (a) $\xi = 0.01$ (b) $\xi = 0.5$. . . 27
17 Streamline patterns for uniform flow past a sphere with radius $a = 1$, $\delta = .001$ and $\delta = 5$: (a) $\xi = 0$ (b) $\xi = .01$ (c) $\xi = 1$. . . 32
18 Stream function portrait for uniform flow in three-dimensions: (a) $\delta = .001$ and $\xi = 0$ (b) $\delta = 5$ and $\xi = 1$. 33
19 Variation of $u_\theta(r)$ with r: (a) $\delta = 1$ (b) $\delta = 5$ (c)$\xi = 0$ (d)$\xi = 0.5$. 34
20 Variation of $\tau_{r\theta}$ with θ: (a) $\delta = 1$ (b) $\xi = 0$. 35
21 Variation of $p(r)$ with r while $\theta = 0^o$: (a) $\delta = 0.1$ (b) $\delta = 1$. . . 36
22 Variation of ω with r where $\theta = \frac{\pi}{2}$: (a) $\xi = .01$ (b) $\xi = 0.5$. . . 37
23 Streamline patterns for shear flow past a sphere with radius $a = 1$, $\delta = .001$: (a) $\xi = 0$ (b) $\xi = 0.5$ (c) $\xi = 1$ and $\xi = 0.5$: (d) $\delta = 0.1$ (e) $\delta = 0.5$ (f) $\delta = 1$. 40
24 Stream function portrait for shear flow in three-dimensions: (a) $\delta = .001$ and $\xi = 0$ (b) $\delta = 1$ and $\xi = 0.5$. 40
25 Variation of u_θ with r: (a)$\delta = 1$ (b)$\delta = 5$. 41
26 Variation of $\tau(r)$ with θ: (a) $\delta = 1$ (b) $\xi = 0$. 42
27 Variation of $p(r)$ with r where $\theta = 0^o$: (a) $\delta = 0.1$ (b) $\delta = 1$. . 43
28 Variation of ω with r where $\theta = \frac{\pi}{4}$: (a) $\xi = 0.01$ (b) $\xi = 0.5$. . 44

29 Variation of F for the uniform flow past a cylinder with: (a) δ for a fixed ξ (b) ξ for a fixed δ. 46
30 Variation of F for the uniform flow past a sphere with: (a) δ for a fixed ξ (b) ξ for a fixed δ. 47

Nomenclature

r	polar radius
a	radius of the cylinder/sphere
$\mathbf{u}$	velocity vector
u_θ	tangential velocity component
u_r	normal velocity component
p	pressure
p_0	pressure's integration constant
k	permeability
∇^2	Laplacian operator in polar coordinates
I_0, I_1, I_2	modified Bessel function of first kind of order 0, 1, 2
K_0, K_1, K_2	modified Bessel function of second kind of order 0, 1, 2
D^2	Laplacian operator in spherical coordinates
$I_{\frac{1}{2}}, I_{\frac{3}{2}}, I_{\frac{5}{2}}$	modified Bessel function of first kind of order $\frac{1}{2}, \frac{3}{2}, \frac{5}{2}$
$K_{\frac{1}{2}}, K_{\frac{3}{2}}, K_{\frac{5}{2}}$	modified Bessel function of second kind of order $\frac{1}{2}, \frac{3}{2}, \frac{5}{2}$
$P_n(\cos(\theta))$	Legendre's functions of the first kind of order n
A, B, C, D, E, M, N	integration constants
$F_{\tau_{rr}}$	force due to normal stress
$F_{\tau_{r\theta}}$	force due to tangential stress
F	total force

Greek symbols

θ	polar angle
μ	viscosity
μ^*	bulk viscosity of the porous media
δ	effective permeability parameter
ψ	Stokes stream function
ξ	slip coefficient
ϕ	spherical azimuthal angular
$\gamma, \beta, \eta, \lambda$	constants involving ξ and δ
α	two-dimensional shear flow constant
$\tau_{r\theta}$	tangential stress in radial and angular direction
ω	vorticity

Abstract

Flow past a circular cylinder or a sphere embedded in a porous medium is investigated mathematically by treating porous matrix as an incompressible fluid. Closed form analytic solutions for the fourth order scalar boundary-value problems for $\psi(r, \theta)$ - known as the Stokes stream function - are obtained by using Navier-slip conditions. Our exact results for $\psi(r, \theta)$ capture flow fields prevailing in the vicinity of a cylinder/sphere suspended in a uniform or a shear flow field. All the physical quantities computed from our solutions depend on two key parameters, namely, δ (the effective permeability) and ξ (slip coefficient). Flow separation and velocity overshoot behavior are found for certain values of δ and ξ. The force acting on the cylinder/sphere is calculated in each case. It is observed that the presence of slip decreases the force on the boundary. Our results show that in the limit $\delta \to 0$, there is no solution to the two-dimensional boundary-value problem, confirming the familiar Stokes paradox.

Acknowledgement[1]

This experience has taught me so much and has allowed me to embrace growth fully. My capacity to become someone; to realize my full potential has become a particular gift for me during this whole journey. My gratitude first goes out to God whom I trusted the most during the whole process; the one who has given me power and strength beyond all that I could imagine; the one from whom I looked up support to in prayers, hoping he would grant me the focus and the determination that I needed to complete everything in full recognition of excellence.

To my advisor, Dr. Devanayagam Palaniappan, I give all the acknowledgements I could think of, especially in helping me out to handle the technical matters of this activity; giving me a better vision of what I was doing, allow me to see things more thoroughly for the sake of improving the way I deal with the issues that I had to come through during the whole process of completing this Thesis.

To all my instructors and the committee members namely, Dr. Diane Denny and Dr. Dugan Um, who believed enough that I can accomplish what I wanted to accomplish out of this program, I give thanks. Their efforts and the time they have spent with students like myself provides me with the proper foundation of self-trust and self-confidence that helped me find a better sense of myself and my capacities; allowing me to grow further into the responsible being that I am today. Special thanks to Dr. Beta Zimmer, who has faith in me, supported and encouraged me permanent. I have learned a lot and I still aspire to learn more from her.

To my family, my father, I thank so much for giving me lifes most precious lessons that I used in order to hold on to my dreams and become focused on matters such as this one for me to get a step closer to my lifes ambition. To my mother who never stopped caring for me and our family; allowing me to focus more on my work and have lesser concerns on other matters that she made sure was accomplished accordingly. To my siblings, Farraj, Dalal, Ahmed, and Ghayda, to my son, Abdurrahman, who always giving me the inspiration to pull through with these activities not only for my personal satisfaction but for the familys growth as well. I could have never done it without them.

To my classmates spacially Douglas Johnson and Chris Trombley and friends, I will never forget how they tried to ease me out whenever I am about to lose my sanity; thanks for being there for making matters a little bit easier to handle even at the breaking point. I will never forget the memories and the lessons I learned from these individuals.

[1]Special thanks to the King Abdullah Foreign Scholarship Program under the supervision of the Saudi Ministry of Education - Higher Education for giving me a chance to embrace a part of my dream and see it becomes a reality.

1 Introduction

Fluid flow involving solids in a porous media has been an area of intensive investigation for the past several decades. The growing emphasis on effective granular and fibrous insulation systems, for the successful containment of transport of radio-nuclide from deposits of nuclear waste materials, stimulated various studies in fluid saturated porous media. Numerous results have been obtained for flow in and around fundamental geometries of interest such as cavities, annulus, and so on. Flow in a porous medium is also important in other practical situations including groundwater movement, catalytic reactors, thermal insulation, oil and gas recovery [7] and drag delivery systems [17]. Several researchers [11] [13] [14] [16] identified many applications that highlight the directions where further theoretical/experimental developments and investigations are required.

Theoretical models describing flow around solid inclusions embedded in a porous medium are based on a variety of partial differential equations (PDEs). Typical model equations connect the physical quantities such as the velocity $\mathbf{u}$ and pressure p. In addition, the parameters including the viscosity μ and permeability k are introduced as necessary. Moreover, the presence of boundaries requires a variety of constraints dictated by practical situations. In order to calculate various physical characteristics of flows, one has to use a unified mathematical technique that describes structures reflected by different physical parameters.

In this thesis, our primary goal is to derive mathematical results for velocity and pressure fields for flows around cylinder and/or a sphere in porous medium. Specifically, we determine analytic solutions for several mathematical boundary-value problems for the higher order PDEs subject to the so called 'slip boundary' condition that has not been effectively utilized in the porous

media context in the literature. After achieving this goal, we use our mathematical results to provide physical characteristics of the flow in a permeable medium involving solid inclusions.

A practical example of the flow around solid inclusions embedded in a

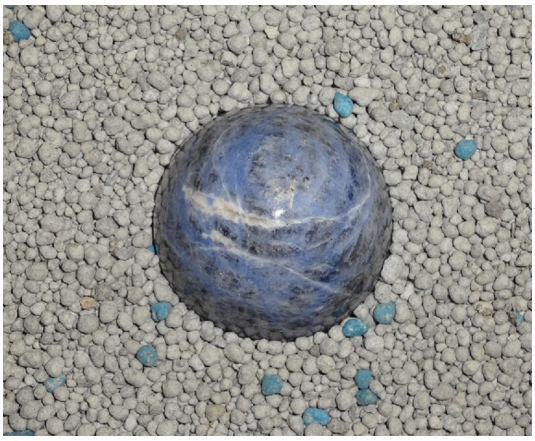

Figure 1: A sample physical model for flow past a solid inclusion in a porous medium.

porous medium is shown in Figure 1. The smaller fine particle-like matrix is the porous/permeable medium and the bigger circular/spherical configuration is solid inclusion. As seen from the figure that the inclusion is suspended in a porous matrix. It is assumed that the permeable material is continuous so the constitutive equations in continuum theory can be applied. With this assumption, the porous medium can be treated as the flow of an incompressible fluid in the viscosity of solid boundaries. We treat circular and spherical inclusions here so that convenient plane polar and spherical polar coordinate systems can be employed. Generalizations of our model to arbitrary body shapes can be a subject of future study.

In the literature two types of theoretical models are in great use to describe flow problems that are relevant for this thesis. They are

- the Darcy model [5]

- the Brinkman model [6].

These two models use the continuum hypothesis in fluid dynamics. Additional details for these models are discussed in **chapter 2**. It has been observed that the Brinkman approach is wisely applicable in high porosity systems [11]. Further, the Brinkman model contains the Darcy approach as a particular case limit of small porosity. For this reason, we adapt the Brinkman model of porous media in our analysis. It should be mentioned that our choice of boundary conditions at the surface of inclusions has not been exploited in the literature in the context of porous media.

The organization of the thesis is as follows. We begin with a description of porous media used in our model in **chapter 2**. In particular, more details of Darcy and Brinkman models are given. Navier-slip condition and its use in fluid dynamics is narrated as well. In chapter 3, the governing equations and stream function formulation for two-dimensional Brinkman flows in plane polar coordinates are provided. Exact solutions for uniform and shear flows past a cylinder are determined in **section 3.1** and **section 3.2**. Flow features and physical quantities (velocity, stress, pressure, and vorticity) are documented in the same subsections. Details for corresponding three-dimensional flows are given in **chapter 4**. Analytic solutions flow characteristics, velocity, stress, pressure, and vorticity distributions are discussed in **sections 4.1** and **4.2**, via., graphical illustrations. The force characteristics in two and three-dimensional cases are demonstrated in **chapter 5**. Finally, our main findings are captured in **chapter 6**. Asummary of flow features is also listed (see pp. 48-49).

The symbols and notations used in this thesis are taken from the cited references, a list of symbols with their denotations was provided on page iii. Derivation of general solutions and identities involving Bessel functions are

given in Appendix A, B, and C.

2 Darcy, Brinkman models, and Navier-slip boundary conditions

A porous medium is defined as a material volume consisting of a solid matrix with an interconnected void. Such a medium is mainly characterized by its porosity, defined as ratio of void space to the total volume of the medium. The voids in general can be of different shapes and sizes.[2]. As mentioned in the introduction, the development of transport models in porous media has a bearing in the progress of several applications. These areas of practical interest include geology, chemical reactions, drying and liquid composite moulding, combustion, medical and biological science [8]. In this chapter, we provide a brief discussion of porous models (Darcy and Brinkman) and Navier-slip conditions.

2.1 Darcy model

The initial investigation of flow within porous media was performed by Henry Darcy [5] in 1856. He proposed a relationship between the instantaneous discharge rate through a porous medium, the viscosity of the fluid and the pressure drop over a distance. More specifically, Darcy's law relates linearly the flow velocity to the pressure gradient across the porous medium. Mathematically, this can be represented as

$$\mathbf{u} = -\frac{\mu}{k}\nabla p, \tag{I}$$

$$\nabla \bullet \mathbf{u} = 0. \tag{II}$$

[2]The porous medium is also characterized by its permeability which is the measure of the flow conductivity in the porous medium

where $\mathbf{u}$ is the filtration velocity, p is the pressure, k is the permeability of the porous material and μ is the viscosity. Equation (II) is the incompressibility condition. Darcy's law given in (I) and (II) predicts the flow behavior well as long as p is small and boundaries are not present. In other words, when the permeability k is small then the Darcy model is suitable in practical situations. However, for large k and higher velocities, the Darcy model has been shown inadequate and so extended models have been proposed. One such model that we use in this thesis is the Brinkman model proposed by Brinkman in 1947 [3] [4]. Below we discuss important features about this model.

2.2 Brinkman model

For a large porosity system (large k) and to include boundary effects, Brinkman proposed a model for the flow in a porous media later known as "Brinkman media" [3] [4]. A Brinkman medium is a homogeneous porous medium characterized by a parameter related to the permeability k. The Brinkman equations represent a viscous fluid flow through a cloud of spherical particles whose size is smaller than the characteristic length scalar of the flow, and therefore occupy a negligible volume [6].

Viscous flow in a porous medium is accurately described by the Brinkman equations for incompressible flow, given by

$$\nabla^2\mathbf{u} - \frac{\mu^*}{\mu\, k}\mathbf{u} = \frac{1}{\mu}\nabla p, \tag{III}$$

$$\nabla \bullet \mathbf{u} = 0. \tag{IV}$$

where μ^* is the bulk viscosity of the porous medium. In (III), the Laplacian term is added to Darcy's law to account for the viscous and boundary effects.

A rigourous theoretical justification of Brinkmans equations was given by Tam [15] and later by Lundgren [10]. Mathematically, the difference between Darcy and Brinkman models is the latter uses higher partial derivatives (∇^2) while the former does not. Sometimes (III) and (IV) are also called Darcy-Brinkman equations. Note that (III) and (IV) are vector partial differential equations of second order for the velocity and pressure fields. We use the Brinkman model equations to investigate flow past cylindrical and spherical boundaries. Next we discuss the boundary conditions to be applied at the surface of the solid inclusions.

2.3 Navier-slip boundary conditions

In order to solve the model equations (III) and (IV) in the presence of boundaries, one must employ appropriate boundary conditions. The so called 'no-slip' condition has been used in almost all studies in porous media. According to this, the fluid neither penetrates nor slips across the boundary surface, implying that $\mathbf{u} = 0$ on the boundary. However, as discussed in [9] (for instance), velocity-slip frequently occurs on the body surface. This leads a different boundary condition, namely, the 'Navier-slip' condition which has been used extensively in viscous hydrodynamics [2]. The slip condition can be stated as

i. the normal component of velocity is zero (impenetrability condition).

ii. the tangential velocity is proportional to the tangential stress at the boundary.

The mathematical forms of the aforementioned conditions are given in **chapters 3** and **4**. When the slip coefficient is considered to be small the Navier

condition reduces to no-slip condition.

In the following chapters we will use Brinkman model equations (III) and (IV) subject to the Navier-slip conditions at the inclusion surface. We will see that the second order vector boundary-value problem becomes a fourth order scalar (BVP) via. stream function formulation. The solutions of the BVP yield flow fields that model flow past a cylinder or a sphere embedded in a porous medium.

3 Brinkman flows past a cylinder (Two-dimensional flows)

In this section we determine analytical solutions for some two-dimensional flows past a circular cylinder embedded in a Brinkman medium. To this end, we use a plane polar coordinate system (r, θ) where r is the radial coordinate measured from the center of the cylinder and θ is the angular coordinate measured from the polar axis as shown in Figure 2. For two-dimensional flows, the velocity vector $\mathbf{u}$ has two components that are functions of r and θ. Let $u_r(r, \theta)$, $u_\theta(r, \theta)$ be the radial and tangential velocity components, as in Figure 2. For two-dimensional flow, the governing equations (III) and (IV)

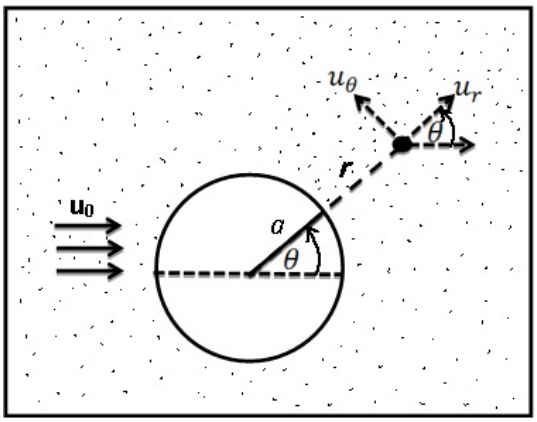

Figure 2: Description of the two-dimensional coordinate system. A steady incompressible flow with the velocity $\mathbf{u}_0$ is due to a basic flow field.

in polar coordinates are written as

$$\left(\frac{\partial^2 u_r}{\partial r^2} + \frac{1}{r}\frac{\partial u_r}{\partial r} + \frac{1}{r^2}\frac{\partial^2 u_r}{\partial \theta^2} - \frac{u_r}{r^2} - \frac{2}{r^2}\frac{\partial u_\theta}{\partial \theta}\right) - \frac{\mu^*}{\mu\, k} u_r = \frac{1}{\mu}\frac{\partial p}{\partial r}, \tag{1}$$

$$\left(\frac{\partial^2 u_\theta}{\partial r^2} + \frac{1}{r}\frac{\partial u_\theta}{\partial r} + \frac{1}{r^2}\frac{\partial^2 u_\theta}{\partial \theta^2} - \frac{u_\theta}{r^2} + \frac{2}{r^2}\frac{\partial u_r}{\partial \theta}\right) - \frac{\mu^*}{\mu\, k} u_\theta = \frac{1}{\mu\, r}\frac{\partial p}{\partial \theta}, \tag{2}$$

$$\frac{\partial}{\partial r}(r u_r) + \frac{\partial u_\theta}{\partial \theta} = 0. \tag{3}$$

Equation (3) is a first order exact partial differential equation. This implies that u_r and u_θ can be derived from a single scalar function, say, $\psi(r,\theta)$ as follows

$$u_r = -\frac{1}{r}\frac{\partial \psi}{\partial \theta} \qquad \text{and} \qquad u_\theta = \frac{\partial \psi}{\partial r}, \tag{4}$$

where the function $\psi(r,\theta)$ is the well-known Stokes stream function used in fluid dynamics. Eliminating the pressure using cross differentiation yields the fourth order partial differential equation for $\psi(r,\theta)$

$$\nabla^4 \psi - \frac{\mu^*}{\mu\, k}\nabla^2 \psi = 0, \tag{5}$$

where ∇^2 is the Laplacian operator given by

$$\nabla^2 \equiv \frac{\partial^2}{\partial r^2} + \frac{1}{r}\frac{\partial}{\partial r} + \frac{1}{r^2}\frac{\partial^2}{\partial \theta^2},$$

in polar coordinates. The solution of (5) subject to suitable boundary conditions will provide the velocity and pressure fields prevailing in the presence of the cylinder with radius $r = a$. The no-slip boundary condition is usually employed in the construction of the solution for various flow fields. However, as discussed in the chapter 2, the no-slip condition is inadequate in many practical situations and indeed there is a slip at the bounding surface [9]. In view of this, we use the Navier slip conditions at the cylindrical surface ($r = a$). These conditions are stated as follows

i. Impenetrability condition: Normal component of velocity is zero ($u_r = 0$).

ii. Slip at the surface: According to [2] [9], the tangential component of the

velocity u_θ is proportional to the tangential stress ($u_\theta = \xi \tau_{r\theta}$), where

$$\tau_{r\theta} = \mu \left[\frac{1}{r} \frac{\partial u_r}{\partial \theta} + r \frac{\partial}{\partial r} (\frac{u_\theta}{r}) \right], \tag{6}$$

In terms of the stream function, the above stated conditions become

$$\psi(a, \theta) = 0, \tag{7a}$$

$$\left. \frac{\partial \psi}{\partial r} \right|_{r=a} = \xi \left. \frac{\partial}{\partial r} \left(\frac{1}{r} \frac{\partial \psi}{\partial r} \right) \right|_{r=a}. \tag{7b}$$

Note that the coefficient of viscosity μ and the radius parameter a have been absorbed in ξ given in equation (7b). Thus, the two-dimensional Brinkman flow past a circular cylinder of radius a reduces to solving a fourth order linear PDE for $\psi(r, \theta)$, equation (5), subject to the set of boundary conditions given in (7). The velocity components can be derived via $\psi(r, \theta)$ using (4), while the pressure is obtained from (1) or (2) after integration. In the following, we derive the exact solutions of two specific profiles, *viz.*, (i) uniform flow (constant velocity at infinity) and (ii) linear shear flow (constant shear at infinity) past a cylinder in Brinkman medium. For future reference, we give here the general solution of (5) in the form

$$\begin{aligned} \psi(r, \theta) = C_0 + D_0 \ln(r) + \sum_{n=1}^{\infty} \Big(C_n \, r^n + D_n \, r^{-n} \Big) \Big(A_n \, \cos(n \, \theta) + B_n \, \sin(n \, \theta) \Big) \\ + \frac{1}{\delta^2} \sum_{n=1}^{\infty} \Big(M_n \, I_n(\delta \, r) - N_n \, K_n(\delta \, r) \Big) \Big(A_n \, \cos(n \, \theta) + B_n \, \sin(n \, \theta) \Big) \end{aligned} \tag{8}$$

where $\delta^2 = \frac{\mu^*}{\mu \, k}$ is the effective permeability parameter. Note that the above solution can be derived using separation of variables in plane polar coordinates. We discuss the uniform flow in **Section 3.1** and linear shear flow in **Section 3.2**.

3.1 Uniform flow past a cylinder

The unbounded velocity field for a uniform flow along x-direction is $\mathbf{u} = u_0\hat{\mathbf{i}}$. The corresponding stream function for the flow is $\psi_0(r,\theta) = r\,\sin(\theta)$ as $r \to \infty$, where we have taken $u_0 = 1$ (unit speed). From (8) we let that $n = 1$, for the uniform flow. This leads to appropriate solution in the presence of the cylinder given by

$$\psi(r,\theta) = \left(r + \frac{D_1}{r} + \frac{M_1}{\delta^2}\,I_1(\delta\,r) - \frac{N_1}{\delta^2}\,K_1(\delta\,r)\right)\,\sin(\theta) \tag{9}$$

where D_1, M_1, N_1 are constants to be determined. Since the perturbed solution must be finite at infinity, we take $M_1 = 0$. Now we use the Navier-slip boundary conditions (7) and the differentiation identities (**see Appendix C, (C-5)-(C-7)**) to determine D_1 and N_1 as

$$N_1 = \frac{-2\delta\left(a^2 + 2\,\xi\right)}{\Big(\left(a^2 + 2\,\xi\right)K_0(\delta\,a) + a\,\xi\,\delta\,K_1(\delta\,a)\Big)} \tag{10a}$$

$$D_1 = -a\left[a + \frac{2\left(a^2 + 2\,\xi\right)}{\delta\,\Big(\left(a^2 + 2\,\xi\right)K_0(\delta\,a) + a\,\xi\,\delta\,K_1(\delta\,a)\Big)}\right] \tag{10b}$$

Finally we arrive to the analytical solution for the uniform flow past a circular cylinder embedded in a porous medium as

$$\psi(r,\theta) = \left[r - \frac{a}{r}\,\beta + \gamma\,K_1(\delta\,r)\right]\,\sin(\theta) \tag{11}$$

where

$$\gamma = \frac{2\big(a^2 + 2\,\xi\big)}{\delta\,\Big(\big(a^2 + 2\,\xi\big)\,K_0(\delta\,a) + a\,\xi\,\delta\,K_1(\delta\,a)\Big)}$$

$$\beta = a + \gamma\,K_1(\delta\,a)$$

When $\xi = 0$, we recover the no-slip flow past a cylinder in Brinkman medium [13] [14]. In the limit of $\xi \to \infty$, (11) becomes

$$\psi(r,\theta) = \Big[r - \frac{a}{r}\Big(a + \frac{4\,K_1(\delta\,a)}{\delta\big(2\,K_0(\delta\,a) + a\,\delta\,K_1(\delta\,a)\big)}\Big) + \frac{4\,K_1(\delta\,r)}{\delta\big(2\,K_0(\delta\,a) + a\,\delta\,K_1(\delta\,a)\big)}\Big]\,\sin(\theta)$$

which is for the pure-slip uniform flow past a cylinder in a porous medium. The analytical solution for $\psi(r,\theta)$ given in (12) is crucial for studying the flow details and physical quantities. In the following subsections, we show some graphical and numerical results for the streamlines patterns, tangential velocity components and shear stress, pressure and vorticity. It is evident from (12) that the stream function and hence all the physical quantities derived from it depend on the two key parameters, namely, (i) the parameter δ, related to the permeability and (ii) the slip-coefficient, ξ. We will provide a discussion of flow fields and related physical quantities based on sample values for δ and ξ. When δ is very small, we find

$$\psi(r,\theta) \sim \Big[\Big(\frac{r}{2} - \frac{1}{2\,r} - r\,\ln(r)\Big)\,\frac{1}{\ln(\delta)} + O(\delta^2)\Big]\,\sin(\theta)$$

this equation becomes zero as $\delta \to 0$. Indeed, we confirm the Stokes paradox; no solution exists for pure Stokes flow across an infinite cylinder. However, our solution (12) does exist for δ small but nonzero.

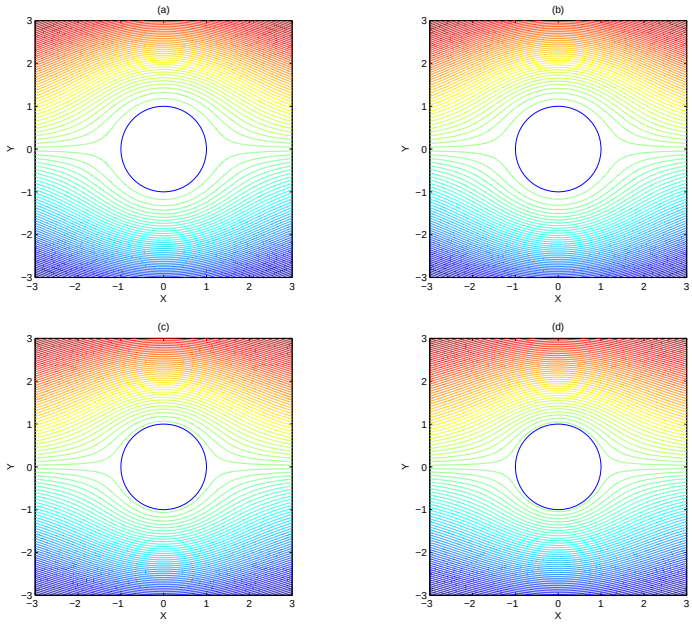

Figure 3: Streamline patterns for uniform flow past a cylinder with radius $a = 1$ and $\delta = .001$: (a) $\xi = 0$ (b) $\xi = .01$ (c) $\xi = .5$ (d) $\xi = 3$.

3.1.1 Streamline patterns

Representative streamline topologies for selected values of δ and ξ are shown in Figure 3 - Figure 6. In general, the streamline patterns are symmetric with respect to x and y axes for various values of δ and ξ. For small values of δ and slip ξ, the behavior is very similar to that of a potential flow around a cylinder [9] under indicial approximation, (see Figure 3(a)). In particular for $\delta = .001$ and $0 \leq \xi \leq .01$, the flow lines resemble to that of the no-slip flow predicted in [13]. This scenario is shown in Figure 3(a)-(b). When $\xi \geq .01$, the streamlines get crowded close to the cylinder as seen in Figure 3(c)-(d). This trend continues for higher values of the slip coefficient as well (not shown here). Next for the large δ, say $\delta = 5$, the streamlines start to become denser close to the cylinder even for $\xi = 0$ (no-slip, Figure 4(a)) and $\xi = 0.01$ (small

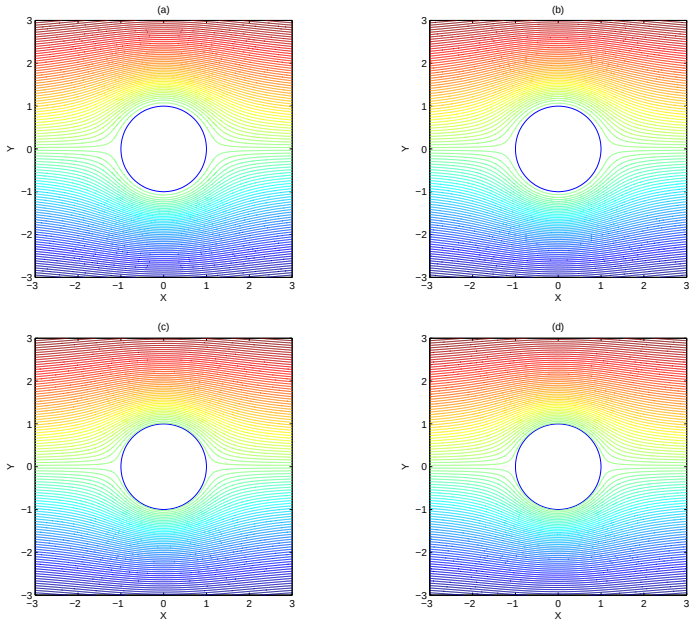

Figure 4: Streamline patters for uniform flow past a cylinder with radius $a = 1$ and $\delta = 5$: (a) $\xi = 0$ (b) $\xi = .01$ (c) $\xi = .5$ (d) $\xi = 3$.

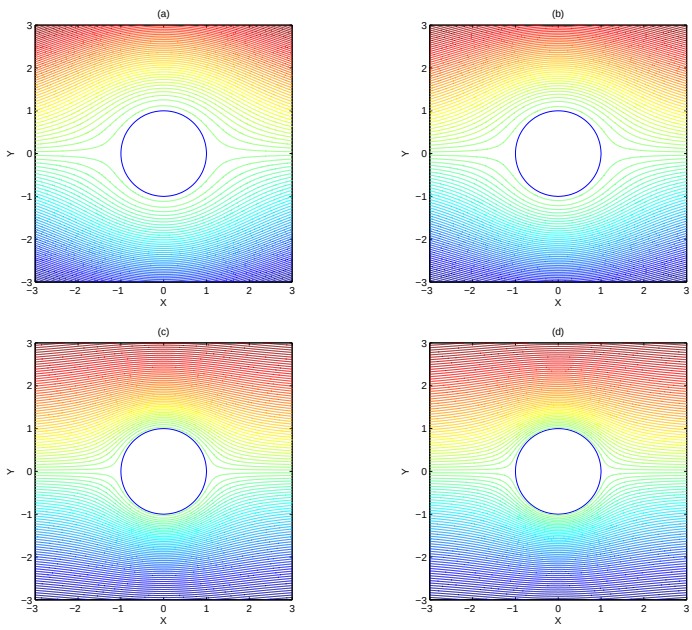

Figure 5: Streamline patterns for uniform flow past a cylinder with radius $a = 1$ and $\xi = .1$: (a) $\delta = .01$ (b) $\delta = .5$ (c) $\delta = 5$ (d) $\delta = 100$.

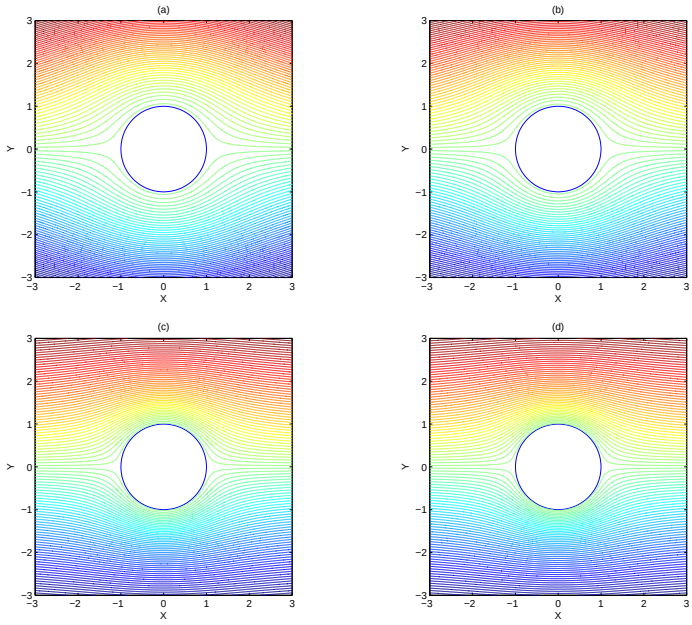

Figure 6: Streamline patterns for uniform flow past a cylinder with radius $a = 1$ and $\xi = .7$: (a) $\delta = .01$ (b) $\delta = .5$ (c) $\delta = 5$ (d) $\delta = 100$.

slip, Figure 4(b)). Further increase of slip increases the contours close to the cylinder as evidenced in Figure 4(c)-(d). Figures 5 and 6 portray streamlines topologies for various values of δ with $\xi = 0.1$ and $\xi = 0.7$, respectively. For low value of δ, the streamlines are intense in the neighborhood of the cylinder as before. The same scenario continues for the increase of δ as seen in Figure 5(a)-(d). When $\xi = 0.7$, the behavior is similar as shown in Figure 6(a)-(d). In all cases, there are two separated region that are symmetric with respect to two coordinate axes.

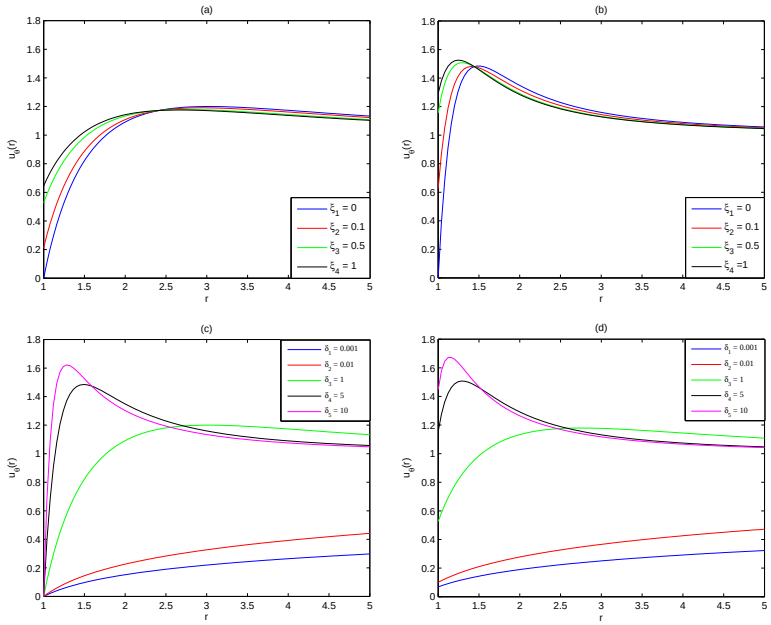

Figure 7: Variation of u_θ with r: (a) $\delta = 1$ (b) $\delta = 5$ (c) $\xi = 0$ (d) $\xi = 0.5$.

3.1.2 Tangential velocity and shear stress

Using (4), the velocity components are obtained as

$$u_r = \left[-1 + \frac{a}{r^2}\,\beta - \frac{\gamma}{r}\,K_1(\delta\, r)\right] \cos(\theta) \tag{13a}$$

$$u_\theta = \left[1 + \frac{a}{r^2}\,\beta - \gamma\delta\, K_0(\delta\, r) - \frac{\gamma}{r}\,K_1(\delta\, r)\right] \sin(\theta) \tag{13b}$$

Notice that that for $\theta = 0$ and $\theta = \pi$ the tangential velocity component vanishes while for $\theta = \frac{\pi}{2}$ and $\theta = \frac{3\pi}{2}$ the normal velocity component u_r is zero. It is of some interest to investigate the behavior of u_θ in detail. For $\theta = \frac{\pi}{2}$, the tangential velocity is plotted versus δ and ξ in Figure 7. It is seen that for $\delta = 1$, u_θ increases up to a maximum value for each ξ and then steadily approach a constant value as r increases in Figure 7(a). It is interesting that the maximum value depends on the slip coefficient ξ, and is greatest when $\xi = 0$ (no-slip). When $\delta = 5$, the behavior of u_θ is more interesting. As in the previous case, u_θ increases up to a maximum value before approaching

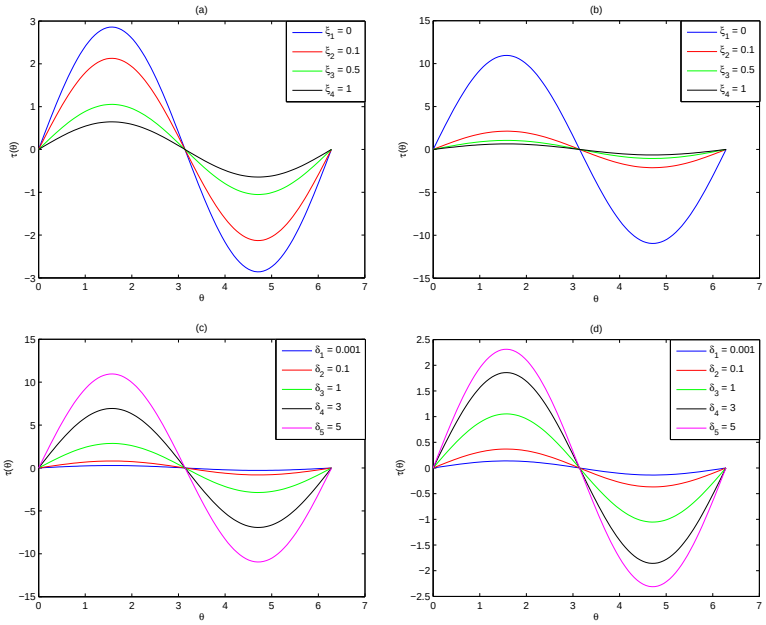

Figure 8: Variation of $\tau_{r\theta}$ with θ: (a) $\delta = 1$ (b) $\delta = 5$, (c) $\xi = 0$ (d) $\xi = 0.5$.

a steady value for greatest r (see Figure 7(b)). But the maximum depends on ξ in an opposite manner. That is, the maximum is low when $\xi = 0$ (no-slip) and is higher as ξ increases. Furthermore, there is a velocity overshoot behavior as can be seen in Figure 7(b). This feature, also observed in no-slip case [13], is significantly influenced by the slip ξ. In fact, large ξ leads to reduce the overshoot to some extent. It should be mentioned that the velocity overshoot occurs at small distance from the cylinder. It is clear that the velocity overshoot occurs which depends on both δ and ξ as shown in Figure 7(c)-(d). When δ is very small, the peak in u_θ is not as high as in case when δ is large.

Shear stress that can be derived from equation (6), is

$$\tau_{r\theta} = \mu\Big[\frac{-4a}{r^3}\beta + \frac{2\gamma\delta}{r}\,K_0(\delta\, r) + \gamma\delta^2\, K_1(\delta\, r) + \frac{4\gamma}{r^2}\,K_1(\delta\, r)\Big]\,\sin(\theta) \qquad (14)$$

The plots of tangential stress versus θ on the surface of the cylinder are shown

in Figure 8 for various δ and ξ. Notice that the changes in effective permeability of and slip simply alters the amplitude of the sine curve. When $\delta = 1$, the amplitude is larger to $\xi = 0$ (no-slip) and smaller for the $\xi = 1$ case. So, $\tau_{r\theta}$ increases monotonically up to a maximum, $\tau_{r\theta} \approx 2.859$ which occurs at $\theta = \frac{\pi}{2}$, for $\xi = 0$. The tangential stress star decreasing and become zero at $\theta = \pi$. The opposite scenario occurs in the lower half when $\pi \leq \theta \leq 2\pi$. Here $\tau_{r\theta}$ decreases to a minimum value of $\tau_{r\theta} \approx -2.859$ at $\theta = \frac{3\pi}{2}$ for $\xi = 0$ (see Figure 8(a)). The maximum and the minimum values for $\xi = 1$ are $\tau_{r\theta} \approx 0.6454$ and $\tau_{r\theta} \approx -0.6454$, respectively. From this we can conclude that the tangential stress is zero at the separation points $\theta = 0$ and $\theta = \pi$, positive at $\theta = \frac{\pi}{2}$ (top) and negative at $\theta = \frac{3\pi}{2}$ (bottom). A similar scenario is observed for $\delta = 5$ as seen in Figure 8(b). It can be noticed that the increase of both δ and ξ decreases the value of $\tau_{r\theta}$. Fixing ξ and varying δ results in a similar behavior, as in Figure 8(c)-(d). When $\xi = 0$, $\tau_{r\theta}$ is small for $\delta = 0.001$ and $\tau_{r\theta}$ is higher for $\delta = 5$. The amplitude increases/decreases as δ is higher/lower when $\xi = 0.5$ as well.

3.1.3 Pressure and vorticity for uniform flow past a cylinder

Pressure can be obtained from equation (1) or (2). The pressure equation is

$$p(r,\theta) = p_0 + \mu\delta^2\left(r + \frac{a}{r}\,\beta\right)\,\cos(\theta) \tag{15}$$

where p_0 is the integration constant. After we make some simplification for the pressure expression, we get

$$p(r,\theta) = p_0 + \mu\delta^2\left[r + \frac{a}{r}\left(a + \frac{2\,K_1(\delta\,a)}{\delta\,K_0(\delta\,a)} - \frac{2\,a\,\xi\left(\frac{K_1(\delta\,a)}{K_0(\delta\,a)}\right)^2}{a^2 + 2\xi + a\xi\delta\frac{K_1(\delta\,a)}{K_0(\delta\,a)}}\right)\right]\,\cos(\theta)$$

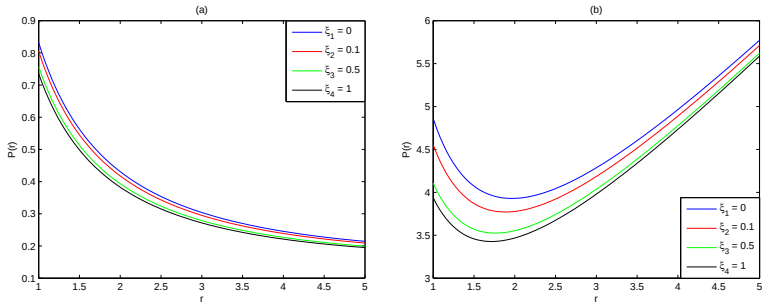

Figure 9: Variation of $p(r)$ with r where $\theta = 0^o$: (a)$\delta = 0.1$ (b)$\delta = 1$.

The plots for the pressure can also be analyzed in a similar way as in tangential velocity and tangential stress. For brevity we omit all the details but provide a short discussion for a couple of values. When $\delta = 0.1$, the pressure is a decreasing function of r. Also, observe that pressure also decreases with increasing ξ (see Figure 9(a)). For $\delta = 1$, the behavior is different in the sense that the pressure decreases up to small r and then increases for greater r in all cases.

The vorticity ω is given the expression

$$\omega = \frac{1}{2}\left(\nabla \times \mathbf{u}\right) \tag{16}$$

where $\nabla \times \mathbf{u}$ in polar coordinates is

$$\nabla \times \mathbf{u} = \frac{1}{r}\Big(\frac{\partial(r\, u_\theta)}{\partial r} - \frac{\partial u_r}{\partial \theta}\Big) \quad \hat{\mathbf{e}_\mathbf{z}}$$

Evaluating, we get

$$\omega = \frac{\delta\,(a^2 + 2\,\xi)\,K_1(\delta\, r)}{(a^2 + 2\,\xi)\,K_0(\delta\, a) + a\,\xi\,\delta\,K_1(\delta\, a)}\,\sin(\theta) \quad \hat{\mathbf{e}_\mathbf{z}} \tag{17}$$

When ξ is fixed, the vorticity decreases until it vanishes far away from the cylinder wall ($r \to \infty$) in Figure10. When $\delta \ll 1$, the rate of change of vor-

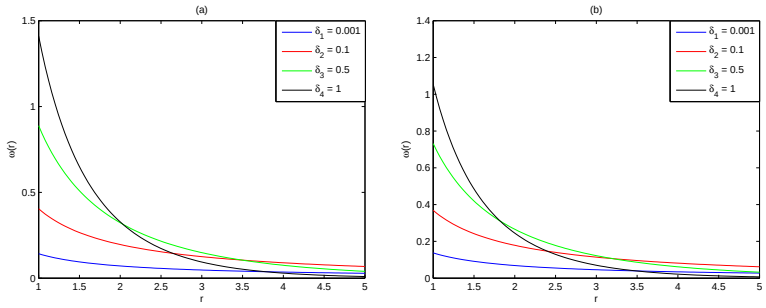

Figure 10: Variation of ω with r where $\theta = \frac{\pi}{2}$: (a)$\xi = 0.01$ (b)$\xi = 0.5$.

ticity is very small but when $\delta \approx 1$, the rate of change increases. From Figure 10(a)-(b), one can see that increasing ξ decreasing the vorticity.

3.2 Shear flow past a cylinder

The stream function for the shear flow past a circular cylinder with radius $r = a$ is $\psi_0(r, \theta) = \alpha\, r\, \sin(\theta)\, \cos(\theta)$ as $r \to \infty$ where $n = 2$ in the general solution (8). The exact solution in presence of cylinder is

$$\psi(r, \theta) = \left(\alpha\, r^2 + \frac{D_2}{r^2} + \frac{M_2}{\delta^2}\, I_2(\delta\, r) - \frac{N_2}{\delta^2}\, K_2(\delta\, r) \right) \sin(\theta)\, \cos(\theta) \tag{18}$$

where D_2, M_2, and N_2 are unknown constants. Using the Navier slip the conditions (7) imposes us to take $M_2 = 0$. Applying the boundary condition (7) and the differentiation identities (**see Appendix C**) in (18) gives D_2 and N_2 as

$$N_2 = \frac{-4\alpha a \delta \big(a^2 + 2\,\xi\big)}{\Big[\big(a^2 + 2\,\xi\big)\, K_1(\delta\, a) + a\xi\delta\, K_2(\delta\, a)\Big]} \tag{19a}$$

$$D_2 = -a^3 \alpha \left[a + \frac{4\big(a^2 + 2\,\xi\big)}{\delta\Big(\big(a^2 + 2\,\xi\big)\, K_1(\delta\, a) + a\xi\delta\, K_2(\delta\, a)\Big)} \right] \tag{19b}$$

Now the analytical solution for the shear flow past a cylinder submerged in a Brinkman medium is

$$\psi(r,\theta) = \left[\alpha\, r^2 - \frac{a^3\alpha}{r^2}\,\beta + a\alpha\,\gamma\, K_2(\delta\, r)\right] \sin(\theta)\, \cos(\theta) \tag{20}$$

where

$$\gamma = \frac{4\big(a^2 + 2\,\xi\big)}{\delta\Big(\big(a^2 + 2\,\xi\big)\, K_1(\delta\, a) + a\,\xi\,\delta\, K_2(\delta\, a)\Big)}$$

$$\beta = a + \gamma\, K_2(\delta\, a)$$

In the limit of $\xi \to \infty$, (20) becomes

$$\begin{aligned}\psi(r,\theta) \;\; &= \left[\alpha\, r^2 - \tfrac{a^3\alpha}{r^2}\left(a + \frac{8\, K_2(\delta\, a)}{\delta\Big(2\, K_1(\delta\, a) + a\,\delta\, K_1(\delta\, a)\Big)}\right)\right. \\ &\quad \left. + \frac{8\, a\,\alpha\, K_2(\delta\, r)}{\delta\Big(2\, K_1(\delta\, a) + a\,\delta\, K_2(\delta\, a)\Big)}\right] \sin(\theta)\, \cos(\theta)\end{aligned}$$

which is for the pure-slip shear flow past a cylinder in a porous medium.

3.2.1 Streamline patterns

Representative streamline topologies for selected values of δ and ξ are shown in Figure 11 - Figure 12. In general, the streamlines patterns are symmetric with respect to x and y axes. For small values of δ and slip ξ, in particular for $\delta = .001$ and $0 \leq \xi \leq .01$, the flow lines are not close to the cylinder wall. This scenario is shown in Figure 11(a). When $\xi > .01$, the streamlines crowd around the cylinder. This trend continues for higher values of the slip coefficient as seen in Figure 11(b)-(c). Next for larger δ, the streamlines start to become denser close to the cylinder even for $\xi = 0$ (no-slip) as seen in Fig-

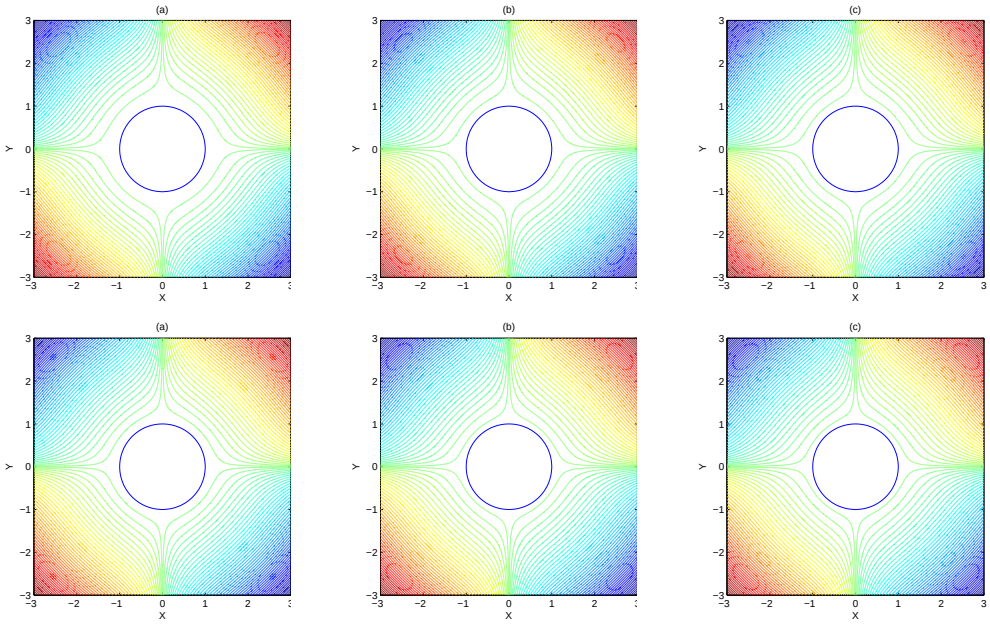

Figure 11: Streamline patterns for shear flow past a circular cylinder with a radius $a = 1$, $\delta = .001$ and $\delta = 5$: (a) $\xi = 0$ (b) $\xi = .5$ (c) $\xi = 1$.

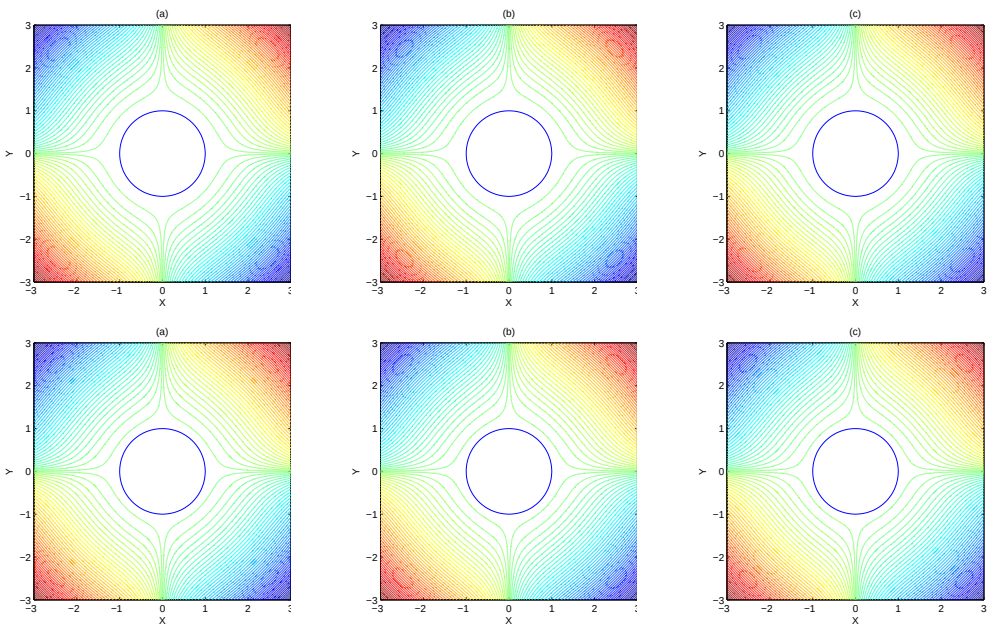

Figure 12: Streamline patterns for shear flow past a circular cylinder with a radius $a = 1$, $\xi = .1$ and $\xi = 0.5$ (a) $\delta = .1$ (b) $\delta = .5$ (c) $\delta = 1$.

ure 11(d). This behavior remains for small slip including $\xi = 0.5$ and $\xi = 1$ from Figure 11(e)-(f). Further increase of slip forces the contours closer to the cylinder as evidenced in Figure 11(c). Figure 12 portrays streamline topologies for various values of δ with $\xi = 0.1$ and $\xi = 0.5$, respectively. For low values of δ, the streamlines are intense in the neighborhood of the cylinder as before. The same scenario continues for the increase of δ as seen in Figure 12(a)-(c). When $\xi = 0.5$, the behavior is similar as shown in Figure 12(d)-(f). In all cases, there are four separated regions that are symmetric with respect to two coordinate axes.

3.2.2 Tangential velocity and shear stress

From equation (4), the velocity components can be obtained as

$$u_r = \Big[-\alpha\, r + \frac{a^3\alpha}{r^3}\,\beta - \frac{a\alpha\gamma}{r}\,K_2(\delta\, r)\Big]\,\big(\cos^2(\theta) - \sin^2(\theta)\big) \tag{22a}$$

$$u_\theta = \Big[2\alpha\, r + \frac{2a^3\alpha}{r^3}\,\beta - a\alpha\gamma\delta\, K_1(\delta\, r) - \frac{2a\alpha\gamma}{r}\,K_2(\delta\, r)\Big]\,\sin(\theta)\,\cos(\theta) \tag{22b}$$

where γ and β as defined in **Section 3.2**. Notice that that for $\theta = 0$, $\theta = \frac{\pi}{2}$, $\theta = \pi$, and $\theta = \frac{3\pi}{2}$ the tangential velocity component vanishes while for $\theta = \frac{\pi}{4}$, $\theta = \frac{3\pi}{4}$, $\theta = \frac{5\pi}{4}$, and $\theta = \frac{7\pi}{4}$ the normal velocity component u_r is zero. The behavior of u_θ can be explored in detail. For $\theta = \frac{\pi}{4}$, the tangential velocity is plotted versus δ and ξ in Figure 13. It is seen that for $\delta = 1$, u_θ increases up to infinity for each ξ in Figure 13(a). When $\delta = 5$, the behavior of u_θ is more interesting. As in the previous case, u_θ increases up to intersection point before approaching infinity for greatest r (see Figure 13(b)). The same manner depends on ξ in Figure 13(c)-(d).

Shear stress that can be derived from equation (6), takes the form

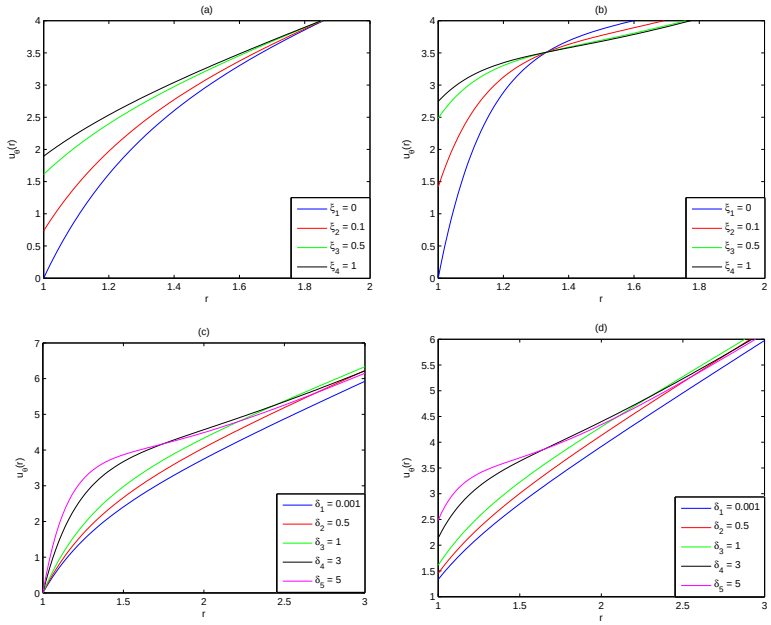

Figure 13: Variation of u_θ with r: (a) $\delta = 1$ (b) $\delta = 5$ (c) $\xi = 0$ (d) $\xi = 0.5$.

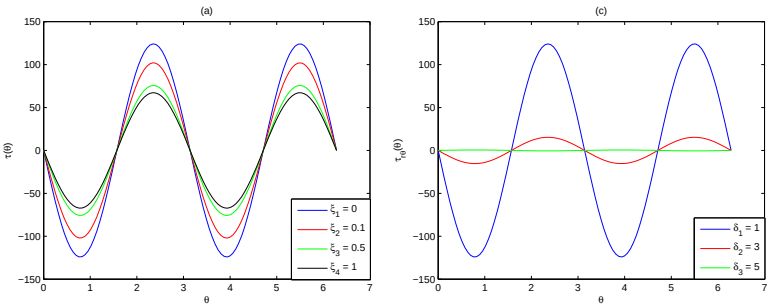

Figure 14: Variation of $\tau_{r\theta}$ with θ: (a) $\delta = 1$ (b) $\xi = 0$.

$$\tau_{r\theta} = \mu\Big[4\alpha - \frac{12a^3\alpha}{r^4}\beta + \frac{2a\alpha\gamma\delta}{r}\,K_1(\delta\, r) + a\alpha\gamma\delta^2\,K_2(\delta\, r) + \frac{12a\alpha\gamma}{r^2}\,K_2(\delta\, r)\Big]\,\sin(\theta)\,\cos(\theta)$$

The plots of tangential stress versus θ on the surface of the cylinder are shown in Figure 14 for various δ and ξ. Notice that the changes in effective permeability and slip influences the amplitude of the trigonometric curve. When $\delta = 1$, the amplitude is larger for $\xi = 0$ (no-slip) and smaller for $\xi = 1$. So, $\tau_{r\theta}$ moves monotonically down to a minimum, $\tau_{r\theta} \approx -124.2$ which occurs at

$\theta = \frac{\pi}{4}$, for $\xi = 0$. It then stars increasing and become zero at $\theta = \frac{\pi}{2}$. The opposite scenario occurs in the upper half when $\frac{\pi}{2} \leq \theta \leq \pi$. Here $\tau_{r\theta}$ increases to a maximum value of $\tau_{r\theta} \approx 124.2$ at $\theta = \frac{3\pi}{4}$ for $\xi = 0$ (see Figure 14(a)). The maximum and the minimum values for $\xi = 1$ are $\tau_{r\theta} \approx 67.18$ and $\tau_{r\theta} \approx -67.18$, respectively. From this we can conclude that the tangential stress is zero at the separation points $\theta = 0$, $\theta = \frac{\pi}{2}$, $\theta = \pi$, and $\theta = \frac{3\pi}{2}$ greater at $\theta = \frac{3\pi}{4}$ and $\theta = \frac{7\pi}{4}$ (top) and smaller at $\theta = \frac{\pi}{4}$ and $\theta = \frac{5\pi}{4}$ (bottom). A similar scenario is observed for higher value of δ. It can be noticed that the increase of both δ and ξ decreases the value of $\tau_{r\theta}$. Fixing ξ and varying δ displays a similar behavior, as in Figure 14(b). When $\xi = 0$, $\tau_{r\theta}$ is higher for $\delta = 1$ and $\tau_{r\theta}$ is lower for $\delta = 5$. The amplitude increases/decreases as δ is lower/higher for the higher values of ξ as well.

3.2.3 Pressure and vorticity for shear flow past a cylinder

Pressure can be obtained from equation (1) or (2). The pressure equation is:

$$p(r,\theta) = p_0 + \mu\alpha\delta^2\Big(r^2 + \frac{a^3}{r^2}\,\beta\Big)\,\cos^2(\theta) \tag{23}$$

where p_0 is the integration constant. After some mathematical work on, we get

$$p(r,\theta) = p_0 + \mu\alpha\delta^2\left[r^2 + \frac{a^3}{r^2}\left(a + \frac{4\,K_2(\delta\,a)}{\delta\,K_1(\delta\,a)} - \frac{4\,a\,\xi\left(\frac{K_2(\delta}{K_1(\delta\,a)}\right)^2}{a^2 + 2\xi + a\xi\delta\frac{K_2(\delta\,a)}{K_1(\delta\,a)}}\right)\right]\cos^2(\theta)$$

The plots for the pressure and vorticity have the same behavior as in the uniform flow case. When $\delta = 0.1$, the pressure is a monotonically decreasing function of r. Observe also that pressure decreases with increasing ξ (see Figure 15(a)). For $\delta = 1$, the behavior is very different. The pressure decreases

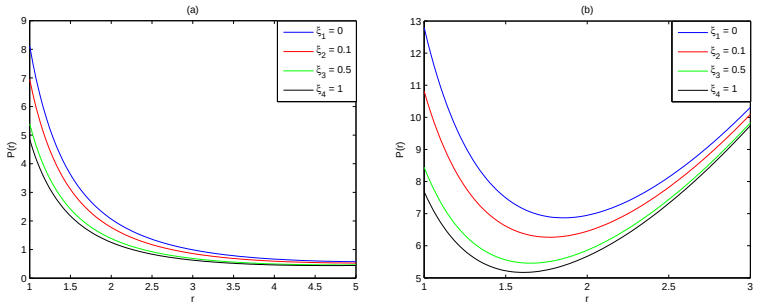

Figure 15: Variation of $p(r)$ with r while $\theta = 0^o$: (a) $\delta = .1$ (b) $\delta = 1$.

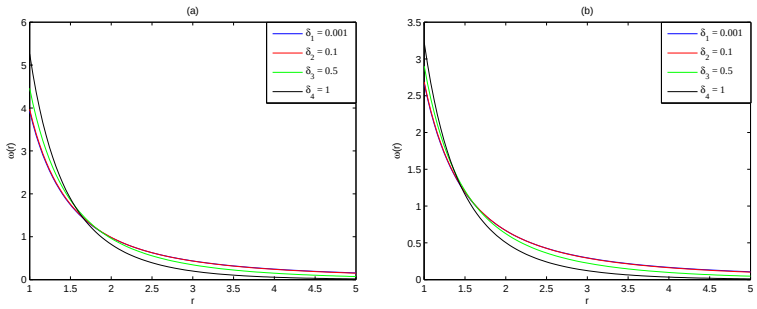

Figure 16: Variation of ω with r while $\theta = \frac{\pi}{4}$: (a) $\xi = 0.01$ (b) $\xi = 0.5$.

for small r and then increases for greater r for any ξ (see Figure 15(a)-(b)). The vorticity ω is obtained from (16)

$$\omega = \frac{2\,a\,\alpha\,\gamma\,\delta\,K_2(\delta\,r)}{(a^2 + 2\,\xi)\,K_1(\delta\,a) + a\,\xi\,\delta\,K_2(\delta\,a)}\,\sin(\theta)\,\cos(\theta)\quad \hat{\mathbf{e}}_{\mathbf{z}} \tag{24}$$

The vorticity, while ξ fixed, decreases until it vanishes far away from the cylinder ($r \to \infty$) as seen in Figure 16. If δ is small, then the rate of change of the vorticity is low. In addition, increasing ξ further reduces the vorticity.

4 Brinkman flows past a sphere (Three-dimensional flows)

Now we consider the flow past a sphere embedded in a porous medium. The mathematical formulation for the three-dimensional flow is very similar to the two-dimensional case discussed in the preceding chapter. For brevity, we provide only the necessary changes in the equations and expressions including notations. We use a spherical coordinate system with coordinates (r, θ, ϕ). Here r is the radial distance measured from the origin, (taken to be at the center of the sphere), and θ and ϕ are the corresponding axial and azimuthal angular coordinates. The flow is assumed to be axisymmetric and so there is no component of the velocity in the azimuthal direction, and therefore all quantities are independent of the coordinate ϕ. Let $u_r(r, \theta)$, $u_\theta(r, \theta)$ be the radial and transverse velocity components of the flow field. The governing equations (III) and (IV) for the three-dimensional flow in terms of the velocity components are

$$\left(\nabla^2 u_r - \frac{2u_r}{r^2} - \frac{2}{r^2}\frac{\partial u_\theta}{\partial \theta} - \frac{2u_\theta \cot\,\theta}{r^2}\right) - \frac{\mu^*}{\mu\, k} u_r = \frac{1}{\mu}\frac{\partial p}{\partial r}, \tag{25}$$

$$\left(\nabla^2 u_\theta - \frac{2}{r^2}\frac{\partial u_r}{\partial \theta} - \frac{u_\theta}{r^2 \sin\,\theta}\right) - \frac{\mu^*}{\mu\, k} u_\theta = \frac{1}{\mu\, r}\frac{\partial p}{\partial \theta}, \tag{26}$$

$$\frac{\partial}{\partial r}(r^2 u_r \sin\,\theta) + \frac{\partial}{\partial \theta}(r u_\theta \sin\,\theta) = 0, \tag{27}$$

where

$$\nabla^2 \equiv \frac{\partial^2}{\partial r^2} + \frac{2}{r}\frac{\partial}{\partial r} + \frac{1}{r^2}\frac{\partial^2}{\partial \theta^2} + \frac{\cot\,\theta}{r^2}\frac{\partial}{\partial \theta}.$$

As we said before, equation (28) is a first order exact partial differential equation. This implies that u_r and u_θ can be derived from a single scalar function,

say $\psi(r,\theta)$, as follows

$$u_r = \frac{1}{r^2 \sin\theta}\frac{\partial\psi}{\partial\theta} \qquad \text{and} \qquad u_\theta = -\frac{1}{r \sin\theta}\frac{\partial\psi}{\partial r}, \tag{28}$$

where $\psi(r,\theta)$ is a Stokes stream function in three-dimensions [12]. Elimination of pressure in (26) and (27) using (29) yields the following fourth order PDE for $\psi(r,\theta)$:

$$D^4\psi - \frac{\mu^*}{\mu\, k} D^2\psi = 0, \tag{29}$$

where D^2 is the axisymmetric Laplacian operator defined by

$$D^2 \equiv \frac{\partial^2}{\partial r^2} + \frac{\sin\theta}{r^2}\frac{\partial}{\partial\theta}\left(\frac{1}{\sin\theta}\frac{\partial}{\partial\theta}\right),$$

in spherical coordinates. As in the two-dimensional case, we apply the impenetrability boundary condition ($u_r = 0$) and the slip condition ($u_\theta = \xi\tau_{r\theta}$) at the surface at the sphere $r = a$, where $\tau_{r\theta}$ given in (6). In terms of Stokes stream function, the boundary conditions become

$$\psi(a,\theta) = 0, \tag{30a}$$

$$\left.\frac{\partial\psi}{\partial r}\right|_{r=a} = \xi\left.\frac{\partial}{\partial r}\left(\frac{1}{r^2}\frac{\partial\psi}{\partial r}\right)\right|_{r=a}, \tag{30b}$$

where ξ is the slip coefficient. Here again, the flow past a sphere reduces to solving a linear PDE, equation (30), subject to the boundary conditions given in (31). The velocity components are derived using (29) while the pressure is computed from (26) or (27). The derivation of the general analytical solution

for (30) is given by

$$\psi(r,\theta) = \sum_{n=0}^{\infty} \left(A_n\, r^{-n} + B_n\, r^{n+1} + \frac{r^{\frac{1}{2}}}{\delta^2} \left(C_n\, I_{n+\frac{1}{2}}(\delta\, r) + D_n\, K_{n+\frac{1}{2}}(\delta\, r) \right) \right) P_n(\cos\,\theta) \tag{31}$$

where $\delta^2 = \frac{\mu^*}{\mu\, k}$ is an effective permeability parameter. With this derivation of the general solution, the analytical solutions for the uniform and shear profile fields in the presence of a sphere installed in a porous medium are obtained.

4.1 Uniform flow past a sphere

Taking $n = 1$ in (32) gives the analytical solution for the uniform profile past a sphere with radius $r = a$. The stream function in this case is $\psi_0(r,\theta) = \frac{1}{2}\, r^2\, \sin^2(\theta)$ as $r \to \infty$. That leads to

$$\psi(r,\theta) = \left(\frac{1}{2}\, r^2 + \frac{A_1}{r} + \frac{r^{\frac{1}{2}} C_1}{\delta^2}\, I_{\frac{3}{2}}(\delta\, r) + \frac{r^{\frac{1}{2}} D_1}{\delta^2}\, K_{\frac{3}{2}}(\delta\, r) \right) \sin^2(\theta) \tag{32}$$

where A_1, C_1, D_1 are constants to be determined. Because the solution must be finite at infinity, we take $C_1 = 0$. As we did in the two-dimensional flows, A_1 and D_1 have been deduced using (33) and the differentiation identities (**see Appendix C**) as follows

$$D_1 = \frac{3a^{\frac{1}{2}}\delta\big(a^3 + 2\xi\big)}{2\Big(\big(a^3 + 2\xi\big) K_{\frac{1}{2}}(\delta\, a) + a\xi\delta\, K_{\frac{3}{2}}(\delta\, a)\Big)} \tag{33a}$$

$$A_1 = -\frac{1}{2} a^2 \left[a + \frac{3\big(a^3 + 2\xi\big) K_{\frac{3}{2}}(\delta\, r)}{\delta\Big(\big(a^3 + 2\xi\big) K_{\frac{1}{2}}(\delta\, a) + a\xi\delta\, K_{\frac{3}{2}}(\delta\, a)\Big)} \right] \tag{33b}$$

Now plugging (34) in (33) to get the final analytic solution for the uniform flow past a sphere embedded in a porous medium as

$$\psi(r,\theta) = \Big(\frac{1}{2}r^2 - \frac{a^2}{2r}\beta + \frac{a^{\frac{1}{2}}\, r^{\frac{1}{2}}\gamma}{2} K_{\frac{3}{2}}(\delta\, r)\Big)\, \sin^2(\theta) \tag{34}$$

where

$$\gamma = \frac{3\big(a^3 + 2\xi\big)}{\delta\Big(\big(a^3 + 2\,\xi\big)\, K_{\frac{1}{2}}(\delta\, a) + a\xi\delta\, K_{\frac{3}{2}}(\delta\, a)\Big)}$$

$$\beta = a + \gamma\, K_{\frac{3}{2}}(\delta\, a)$$

The pure-slip flow ($\xi \to \infty$) is given by

$$\psi(r,\theta) = \left[\frac{1}{2}r^2 - \frac{a^2}{2r}\Big(a + \frac{6\, K_{\frac{3}{2}}(\delta\, a)}{\delta\big(2\, K_{\frac{1}{2}}(\delta\, a) + a\,\delta\, K_{\frac{3}{2}}(\delta\, a)\big)}\Big) + \frac{3\, a^{\frac{1}{2}}\, r^{\frac{1}{2}}\, K_{\frac{3}{2}}(\delta\, r)}{\delta\big(2\, K_{\frac{1}{2}}(\delta\, a) + a\,\delta\, K_{\frac{3}{2}}(\delta\, a)\big)}\right] \sin^2(\theta)$$

(35) can be rewrite using (C-13) and (C-14) as

$$\psi(r,\theta) = \left[\frac{1}{2}r^2 - \frac{\lambda}{2\, r} + \frac{\eta}{2} e^{\delta(a-r)}\Big(\delta + \frac{1}{r}\Big)\right] \sin^2(\theta) \tag{36}$$

where

$$\eta = \frac{3a(a^3 + 2\xi)}{\delta^2\Big(a^3 + 3\xi + a\xi\delta\Big)}$$

$$\lambda = a^3 + \eta\,(\delta\, a + 1)$$

with pure-slip flow is given by

$$\psi(r,\theta) = \left[\frac{1}{2}r^2 - \frac{1}{2\, r}\Big(a^3 + \frac{6\, a\,(\delta\, a + 1)}{\delta^2\,(3 + \delta\, a)}\Big) + \frac{3\, a}{\delta\,(3 + \delta\, a)}\, e^{\delta(a-r)}\Big(1 + \frac{1}{\delta\, r}\Big)\right] \sin^2(\theta)$$

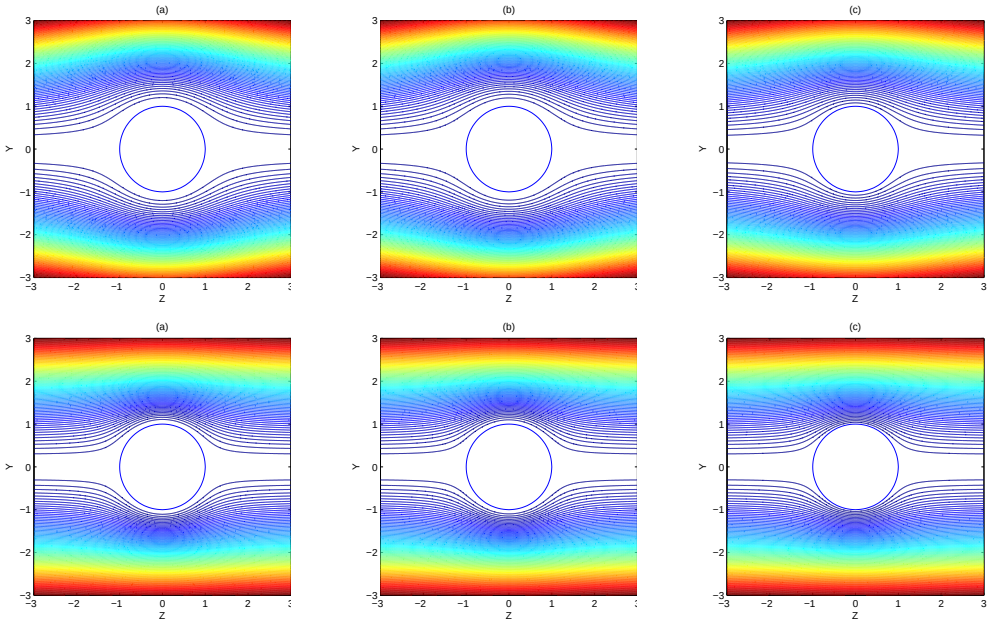

Figure 17: Streamline patterns for uniform flow past a sphere with radius $a = 1$, $\delta = .001$ and $\delta = 5$: (a) $\xi = 0$ (b) $\xi = .01$ (c) $\xi = 1$.

4.1.1 Streamline patterns

Various typical streamline topologies for selected values of δ and ξ are shown in Figure 17. In general, the streamline patterns are symmetric with respect to x and y axes for various values of δ and ξ. For small values of δ and slip ξ, the behavior is very similar to that of a potential flow around a sphere under indicial approximation. In particular for $\delta = .001$ and $0 \leq \xi \leq .01$, the flow lines resemble to that of the no-slip flow predicted in [14]. This scenario is shown in Figure 17(a)-(b). When $\xi > .01$, the streamlines get crowded around to the sphere as seen in Figure 17(c). This trend continues to grow for higher values of the slip coefficient. Next for large δ, the streamlines also start to become denser close to the sphere for ($\xi = 0$) and small slip ($\xi = 0.01$).

Further increase of slip increases the density of contours close to the sphere as evinced in Figure 17(d)-(f). The crowding increasing for the increase of δ and increasing ξ as seen in Figure 17(d)-(f), the behavior is similar to other

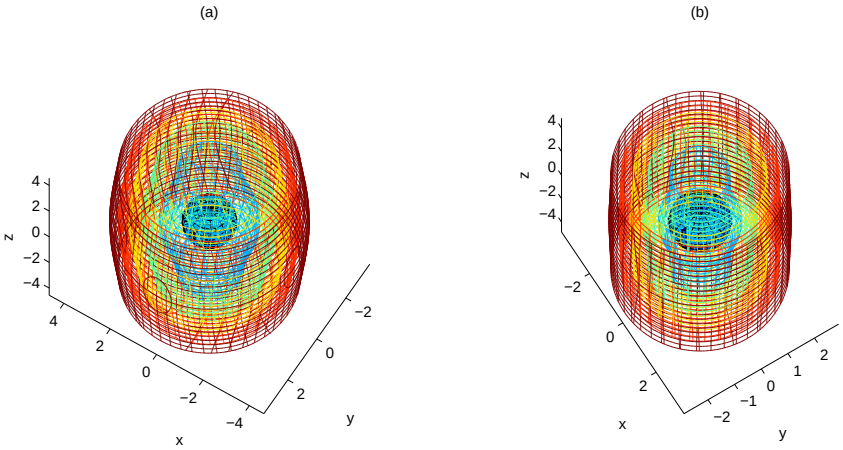

Figure 18: Stream function portrait for uniform flow in three-dimensions: (a) $\delta = .001$ and $\xi = 0$ (b) $\delta = 5$ and $\xi = 1$.

choices of slip coefficient. In all cases, there are two separated region that are symmetric with respect to two coordinate axes. The corresponding stream function portrait in three-dimensions is displayed in Figure 18.

4.1.2 Tangential velocity and shear stress

The velocity components derived from (29) are

$$u_r = \Big[1 - \frac{a^2}{r^3}\beta + \frac{a^{\frac{1}{2}}\gamma}{r^{\frac{3}{2}}}\, K_{\frac{3}{2}}(\delta\, r)\Big]\, \cos(\theta) \tag{38a}$$

$$u_\theta = \Big[-1 - \frac{a^2}{2r^3}\beta + \frac{a^{\frac{1}{2}}\gamma\delta}{2r^{\frac{1}{2}}}\, K_{\frac{1}{2}}(\delta\, r) + \frac{a^{\frac{1}{2}}\gamma}{2r^{\frac{3}{2}}}\, K_{\frac{3}{2}}(\delta\, r)\Big]\, \sin(\theta) \tag{38b}$$

Also, using (C-13) and (C-14) to rewrite the velocity components as

$$u_r = \Big[1 - \frac{\lambda}{r^3} + \eta\, e^{\delta(a-r)}\Big(\frac{\delta}{r^2} + \frac{1}{r^3}\Big)\Big]\, \cos(\theta)$$

$$u_\theta = \Big[-1 - \frac{\lambda}{2r^3} + \frac{\eta}{2}\, e^{\delta(a-r)}\Big(\frac{\delta^2}{r} + \frac{1}{r^2} + \frac{1}{r^3\delta}\Big)\Big]\, \sin(\theta)$$

Notice that that for $\theta = 0$ and $\theta = \pi$ the tangential velocity component

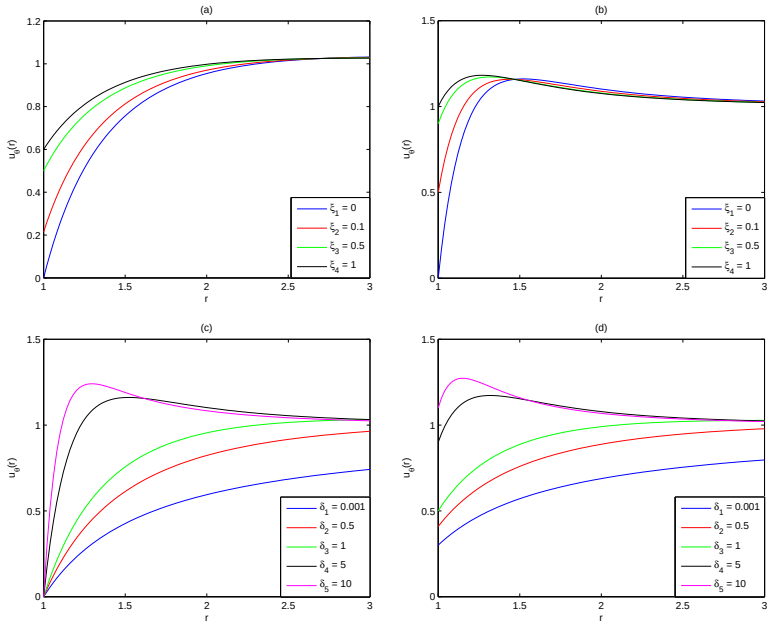

Figure 19: Variation of $u_\theta(r)$ with r: (a) $\delta = 1$ (b) $\delta = 5$ (c)$\xi = 0$ (d)$\xi = 0.5$.

vanishes while for $\theta = \frac{\pi}{2}$ and $\theta = \frac{3\pi}{2}$ the normal velocity component u_r is zero. It is of some interest to investigate the behavior of u_θ in detail. For $\theta = \frac{\pi}{2}$, the tangential velocity is plotted versus δ and ξ in Figure 19. It is seen that for $\delta = 1$, u_θ monotonically increases up to a maximum value independent of ξ and then steadily approach this constant value as r increases in Figure 19(a). When $\delta = 5$, the behavior of u_θ is more interesting. As in the previous case, u_θ increases up to a maximum value independent of ξ before approaching a steady value as $r \to \infty$. Furthermore, there is a velocity overshoot behavior as can be seen in Figure 19(b). This feature, also observed in no-slip case [14], is significantly influenced by the slip ξ. In fact, large ξ leads to minimize the overshoot to some extent. It should be mentioned that the velocity overshoot occurs at a small distance from the sphere. The plots for u_θ versus r for various δ and ξ are shown in Figure 19(c)-(d). It is clear that the velocity overshoot occurs which depends on both δ and ξ as shown in Figure 19(c)-(d). When δ is very small, the peak in u_θ is not as high as in case when δ is large.

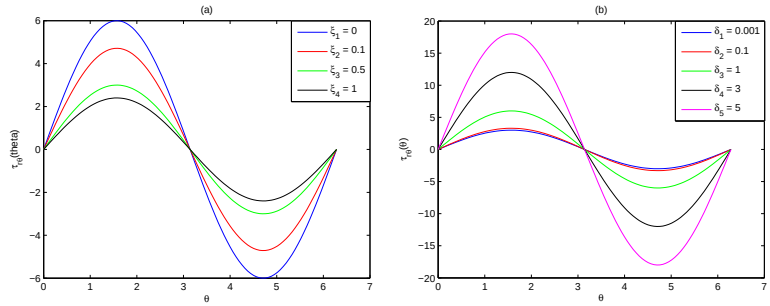

Figure 20: Variation of $\tau_{r\theta}$ with θ: (a) $\delta = 1$ (b) $\xi = 0$.

Shear stress that can be derived from equation (6), is

$$\tau_{r\theta} = \mu\Big[\frac{3a^2}{r^4}\beta - \frac{a^{\frac{1}{2}}\gamma\delta}{r^{\frac{3}{2}}}\,K_{\frac{1}{2}}(\delta\, r) - \frac{a^{\frac{1}{2}}\gamma\delta^2}{2\,r^{\frac{1}{2}}}\,K_{\frac{3}{2}}(\delta\, r) - \frac{3a^{\frac{1}{2}}\gamma}{r^{\frac{5}{2}}}\,K_{\frac{3}{2}}(\delta\, r)\Big]\,\sin(\theta) \quad (40)$$

using (C-13) and (C-14) gives the shear stress in the term of the elementary function:

$$\tau_{r\theta} = \mu\Big[\frac{3\lambda}{r^4} + \frac{\eta}{2}\delta^2\, e^{\delta(a-r)}\Big(\frac{\delta}{r} + \frac{5}{r^2} + \frac{9}{\delta\, r^3} + \frac{10}{r^4\delta^2}\Big)\Big]\,\sin(\theta)$$

As we discussed in the uniform flow in two-dimensions, the changes in effective permeability and slip alters the amplitude of the sine curve. When $\delta = 1$, the amplitude is larger in the $\xi = 0$ (no-slip) case and smaller for $\xi = 1$. $\tau_{r\theta}$ increases monotonically for $0 \leq \theta \leq \pi$ up to a maximum, $\tau_{r\theta} \approx 5.999$ which occurs at $\theta = \frac{\pi}{2}$, for $\xi = 0$. It then stars decreasing and become zero at $\theta = \pi$. An opposite scenario occurs in the lower half when $\pi \leq \theta \leq 2\pi$. Here $\tau_{r\theta}$ decreases to a minimum value of $\tau_{r\theta} \approx -5.999$ at $\theta = \frac{3\pi}{2}$ for $\xi = 0$ (see Figure 20(a)). The maximum and the minimum values for $\xi = 1$ are $\tau_{r\theta} \approx 2.4$ and $\tau_{r\theta} \approx -2.4$, respectively. From this we can conclude that the tangential stress is zero at the separation points $\theta = 0$ and $\theta = \pi$ positive at $\theta = \frac{\pi}{2}$ (top) and negative at $\theta = \frac{3\pi}{2}$ (bottom). A similar scenario is observed for higher value of δ. It can be noticed that the increase of both δ and ξ decreases the value of $\tau_{r\theta}$.

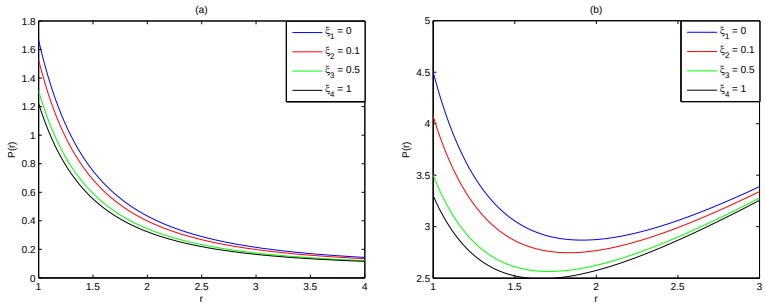

Figure 21: Variation of $p(r)$ with r while $\theta = 0^o$: (a) $\delta = 0.1$ (b) $\delta = 1$.

Fixing ξ and varying δ displays a similar behavior, as in Figure 20(b). When $\xi = 0$, $\tau_{r\theta}$ is small for $\delta = 0.001$ and $\tau_{r\theta}$ is higher for $\delta = 5$. The amplitude increases/decreases as δ is higher/lower when $\xi = 0.5$ as well.

4.1.3 Pressure and vorticity for uniform flow past a sphere

Pressure can be obtained from equation (26) or (27). The pressure equation is:

$$p(r,\theta) = p_0 - \mu\delta^2\Big(r + \frac{a^2}{2r^2}\beta\Big)\,\cos(\theta) \tag{41}$$

where p_0 is the integration constant. Using (C-13) and (C-14) gives

$$p(r,\theta) = p_0 - \mu\delta^2\Big(r + \frac{\lambda}{2r^2}\Big)\,\cos(\theta)$$

After algebraic manipulation of the pressure expressions, we get

$$p(r,\theta) = p_0 - \mu\delta^2\left[r + \frac{a^2}{2\,r^2}\left(a + \frac{3\,K_{\frac{3}{2}}(\delta\,a)}{\delta\,K_{\frac{1}{2}}(\delta\,a)} - \frac{3\,a\,\xi\,\left(\frac{K_{\frac{3}{2}}(\delta\,a)}{K_{\frac{1}{2}}(\delta\,a)}\right)^2}{a^3 + 2\xi + a\xi\delta\frac{K_{\frac{3}{2}}(\delta\,a)}{K_{\frac{1}{2}}(\delta\,a)}}\right)\right]\cos(\theta)$$

$$p(r,\theta) = p_0 - \mu\delta^2\Big(r + \frac{1}{2\,r^2}\Big(a^3 + \frac{3\,a\,(\delta\,a+1)}{\delta^2} - \frac{3\,a\,\xi\,(\delta\,a+1)^2}{\delta^2\,(a^3 + 3\,\xi + a\,\xi\,\delta)}\Big)\Big)\,\cos(\theta)$$

The plots for the pressure and vorticity have the same behavior as in the

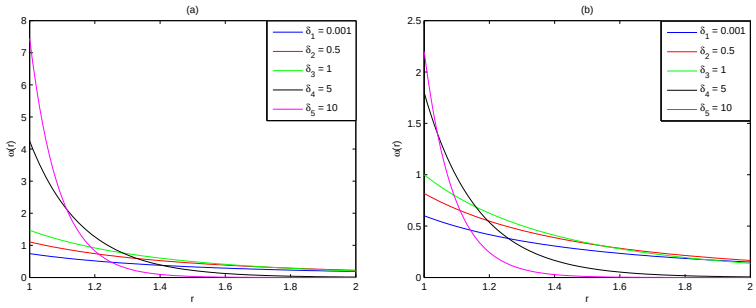

Figure 22: Variation of ω with r where $\theta = \frac{\pi}{2}$: (a) $\xi = .01$ (b) $\xi = 0.5$.

two-dimensional case. When $\delta = 0.1$, the pressure is a decreasing function of r. Observe also that pressure decreases with increasing ξ (see Figure 21(a)). For $\delta = 1$, the behavior is different in the sense that the pressure decreases to a minimum up to small r and then increases for greater r in all cases (see Figure 21(a)-(b)).

The vorticity ω is given by the expression:

$$\omega = \frac{3\, a^{\frac{1}{2}} \delta \left(a^3 + 2\,\xi\right) K_{\frac{3}{2}}(\delta\, r)}{4 r^{\frac{1}{2}} \Big(\left(a^3 + 2\,\xi\right) K_{\frac{1}{2}}(\delta\, a) + a\xi\delta\, K_{\frac{3}{2}}(\delta\, a) \Big)} \sin(\theta) \quad \hat{\mathbf{e}_{\mathbf{z}}} \tag{43}$$

or we can rewrite it using (C-13) and (C-14) as

$$\omega = \frac{3\, a\, (a^3 + 2\xi)}{4(a^3 + 3\xi + a\xi\delta)}\, e^{\delta(a-r)} \left(\frac{\delta}{r} + \frac{1}{r^2} \right) \sin(\theta) \quad \hat{\mathbf{e}_{\mathbf{z}}}$$

Examine the vorticity, keeping δ fixed, we notice that the vorticity decreases untill it vanishes far away from sphere surface ($r \to \infty$) in Figure 22. Also, the change of vorticity is very small when $\delta \ll 1$ but increases as δ rises. Making the same investigation while keeping ξ fixed the vorticity increases with δ. However, the vorticity decreases while as ξ increases (see Figure 22(a)-(b)).

4.2 Shear flow past a sphere

We find that the stream function of the shear flow past a sphere with radius a by taking $n = 2$ in the general solution (32). The asymptotic stream function in spherical coordinates for the shear flow in the three-dimensional plane is $\psi_0(r,\theta) = r^3 \sin^2(\theta) \cos(\theta)$. Therefore, the general form is

$$\psi(r,\theta) = \left(r^3 + \frac{A_2}{r^2} + \frac{r^{\frac{1}{2}} C_2}{\delta^2} I_{\frac{5}{2}}(\delta\, r) + \frac{r^{\frac{1}{2}} D_2}{\delta^2} K_{\frac{5}{2}}(\delta\, r) \right) \sin^2(\theta) \cos(\theta) \tag{44}$$

where A_2, C_2, D_2 are unknown constants. We obtain $C_2 = 0$ by the conditions at infinity. We apply the boundary condition (31) and the differentiation identities (**see Appendix C**) in (45) to get A_2 and D_2 as

$$D_2 = \frac{5a^{\frac{3}{2}}\delta\left(a^3 + 2\xi\right)}{\left(a^3 + 2\xi\right) K_{\frac{3}{2}}(\delta\, a) + a\xi\delta\, K_{\frac{5}{2}}(\delta\, a)} \tag{45a}$$

$$A_2 = -a^4 \left[a + \frac{5\left(a^3 + 2\xi\right) K_{\frac{5}{2}}(\delta\, a)}{\delta\Big(\left(a^3 + 2\xi\right) K_{\frac{3}{2}}(\delta\, a) + a\xi\delta\, K_{\frac{5}{2}}(\delta\, a)\Big)} \right] \tag{45b}$$

The analytic solution for the shear flow past a sphere is therefore given by

$$\psi(r,\theta) = \left[r^3 - \frac{a^4}{r^2}\beta + a^{\frac{3}{2}}\, r^{\frac{1}{2}} \gamma\, K_{\frac{5}{2}}(\delta\, r) \right] \sin^2(\theta) \cos(\theta) \tag{46}$$

where

$$\gamma = \frac{5\left(a^3 + 2\xi\right)}{\delta\Big(\left(a^3 + 2\xi\right) K_{\frac{3}{2}}(\delta\, a) + a\xi\delta\, K_{\frac{5}{2}}(\delta\, a)\Big)}$$

$$\beta = a + \gamma\, K_{\frac{5}{2}}(\delta\, a)$$

In order to simplify the solution, we can use the fact (C-14) and (C-15) to get

$$\psi(r,\theta) = \left[r^3 - \frac{\lambda}{r^2} + \eta\, e^{\delta(a-r)} \Big(\delta^2 + \frac{3\delta}{r} + \frac{3}{r^2} \Big) \right] \sin^2(\theta)\, \cos(\theta) \tag{48}$$

where

$$\eta = \frac{5a^3(a^3+2\xi)}{\delta^2 \Big[(a^3+5\xi)(a\delta+1) + a^2\delta^2\xi \Big]}$$
$$\lambda = a^5 + \eta \Big(\delta^2\, a^2 + 3\,\delta\, a + 3 \Big)$$

This gives pure-slip flow of

$$\psi(r,\theta) = \Bigg[r^3 - \frac{a^4}{r^2} \Big(a + \frac{10\, K_{\frac{5}{2}}(\delta\, a)}{\delta \big(2\, K_{\frac{3}{2}} + a\,\delta\, K_{\frac{5}{2}}(\delta\, a) \big)} \Big) + \frac{10\, a^{\frac{3}{2}}\, r^{\frac{1}{2}}\, K_{\frac{5}{2}}(\delta\, r)}{\delta \big(2\, K_{\frac{3}{2}} + a\,\delta\, K_{\frac{5}{2}}(\delta\, a) \big)} \Bigg] \sin^2(\theta)\, \cos(\theta)$$

or

$$\psi(r,\theta) = \Bigg[r^3 - \frac{1}{r^2} \Big(a^5 + \frac{10\, a^3\, (\delta^2\, a^2 + 3\,\delta\, a + 3)}{\delta^2 (\delta^2\, a^2 + 5\, a\,\delta + 5)} \Big) + \frac{10\, a^3}{\delta^2\, a^2 + 5\, a\,\delta + 5}\, e^{\delta(a-r)} \Big(1 + \frac{3}{\delta\, r} + \frac{3}{\delta^2\, r^2} \Big) \Bigg] \sin^2(\theta)\, \cos(\theta)$$

4.2.1 Streamline Patterns

Representative streamline topologies for selected values of δ and ξ are shown in Figure 23. In general, the streamlines patterns are symmetric with respect to x and y axes and any line in the region for various values of δ and ξ. For small values of δ and slip ξ no topological changes seen with changing ξ have similar behavior. This scenario is shown in Figure 23(a)-(c).

Figure 23(d)-(f) portray streamline topologies for various values of δ with

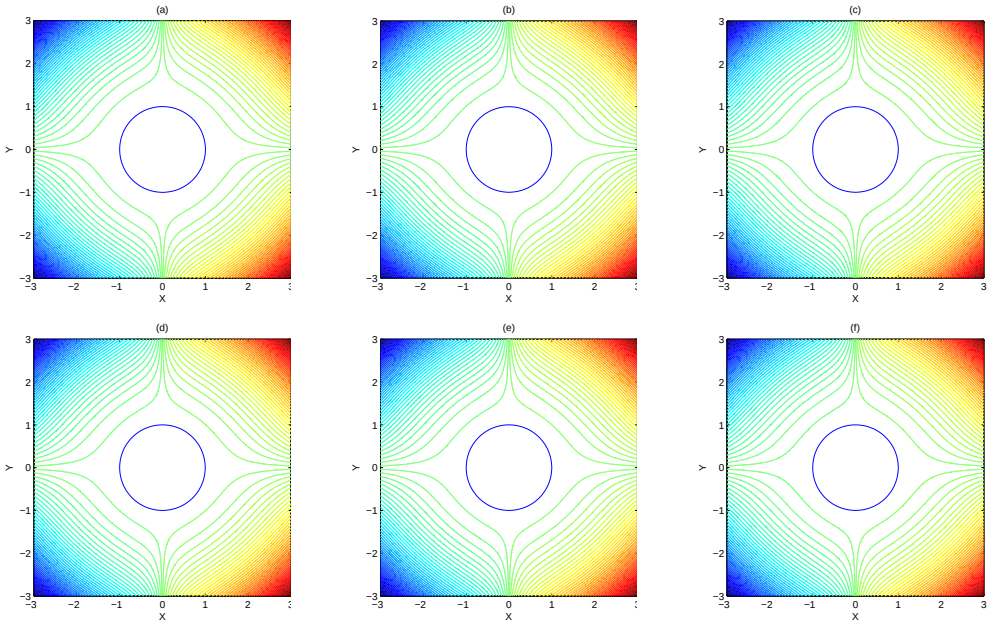

Figure 23: Streamline patterns for shear flow past a sphere with radius $a = 1$, $\delta = .001$: (a) $\xi = 0$ (b) $\xi = 0.5$ (c) $\xi = 1$ and $\xi = 0.5$: (d) $\delta = 0.1$ (e) $\delta = 0.5$ (f) $\delta = 1$.

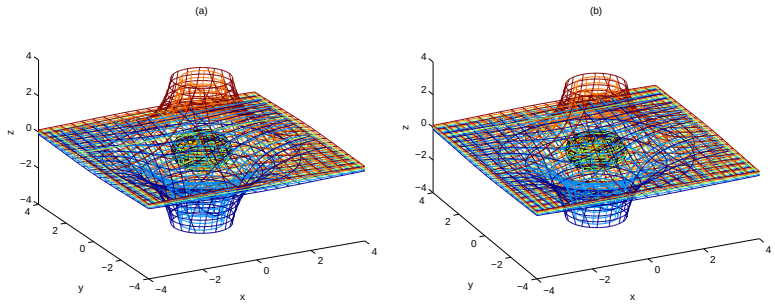

Figure 24: Stream function portrait for shear flow in three-dimensions: (a) $\delta = .001$ and $\xi = 0$ (b) $\delta = 1$ and $\xi = 0.5$.

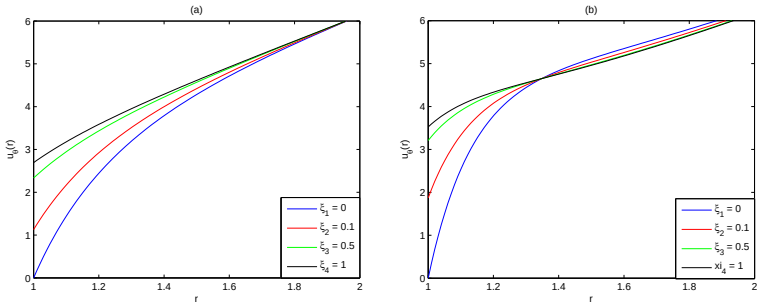

Figure 25: Variation of u_θ with r: (a)$\delta = 1$ (b)$\delta = 5$.

$\xi = 1$ are infinitesimally. In all cases, there are four separated regions that are symmetric with respect to two coordinate axes. The corresponding stream function portrait in three-dimensions is shown in Figure 24.

4.2.2 Tangential velocity and shear stress

The velocity components are obtained from (29) as

$$u_r = \left[r - \frac{a^4}{r^4}\beta + \frac{a^{\frac{3}{2}}\gamma}{r^{\frac{3}{2}}} K_{\frac{5}{2}}(\delta\, r)\right] \left(2\cos^2(\theta) - \sin^2(\theta)\right) \tag{50a}$$

$$u_\theta = \left[-3r - \frac{2a^4}{r^4}\beta + \frac{a^{\frac{3}{2}}\gamma\delta}{r^{\frac{1}{2}}} K_{\frac{3}{2}}(\delta\, r) + \frac{2a^{\frac{3}{2}}\gamma}{r^{\frac{3}{2}}} K_{\frac{5}{2}}(\delta\, r)\right] \sin(\theta)\, \cos(\theta) \tag{50b}$$

Using the expression in (C-14) and (C-15) to rewrite (51)

$$u_r = \left[r - \frac{\lambda}{r^4} + \eta\, e^{\delta(a-r)}\left(\frac{\delta^2}{r^2} + \frac{3\delta}{r^3} + \frac{3}{r^4}\right)\right] \left(2\cos^2(\theta) - \sin^2(\theta)\right)$$

$$u_\theta = \left[-3r - \frac{2\lambda}{r^4} + \eta\,\delta\, e^{\delta(a-r)}\left(\frac{\delta^2}{r} + \frac{3\delta}{r^2} + \frac{6}{r^3} + \frac{6}{r^4\delta}\right)\right] \sin(\theta)\, \cos(\theta)$$

Notice that that for $\theta = 0$, $\theta = \frac{\pi}{2}$, $\theta = \pi$, and $\theta = \frac{3\pi}{2}$ the tangential velocity component vanishes. It is of some interest to investigate the behavior of u_θ in detail. For $\theta = \frac{\pi}{4}$, the tangential velocity is plotted versus δ and ξ in Figure 25. It is seen that for $\delta = 1$, u_θ increases up to infinity for each ξ in Figure

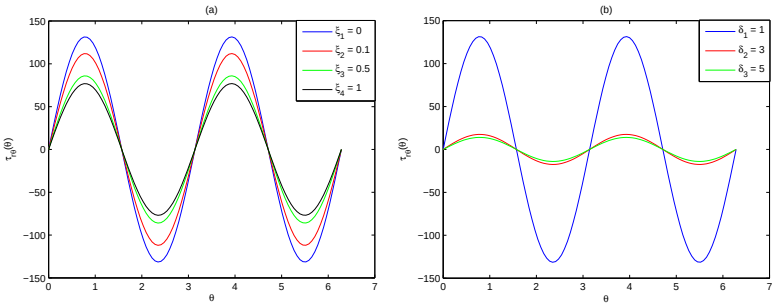

Figure 26: Variation of $\tau(r)$ with θ: (a) $\delta = 1$ (b) $\xi = 0$.

25(a). When $\delta = 5$, as in the previous section, u_θ increases up to intersection point before diverging for large r (see Figure 25(b)).

Shear stress that can be derived from equation (6), is

$$\tau_{r\theta} = \mu\Big[-6 + \frac{16\,a^4}{r^5}\beta - \frac{2\,a^{\frac{3}{2}}\gamma\delta}{r^{\frac{3}{2}}}\,K_{\frac{3}{2}}(\delta\,r) - \frac{a^{\frac{3}{2}}\gamma\delta^2}{r^{\frac{1}{2}}}\,K_{\frac{5}{2}}(\delta\,r) - \frac{16a^{\frac{3}{2}}\gamma}{r^{\frac{5}{2}}}\,K_{\frac{5}{2}}(\delta\,r)\Big]\,\sin(\theta)\,\cos(\theta)$$

using (C-14) and (C-15) gives the shear stress in the term of the elementary function:

$$\tau_{r\theta} = \mu\Big[-6 + \frac{16\lambda}{r^5} - \eta\delta^2\,e^{\delta(a-r)}\Big(\frac{\delta^2}{r} + \frac{5\delta}{r^2} + \frac{21}{r^3} + \frac{48}{r^4\delta} + \frac{48}{r^5\delta^2}\Big)\Big]\,\sin(\theta)\,\cos(\theta)$$

As we discussed in the shear flow in two-dimensions, the changes in effective permeability of and slip simply alters the amplitude of the trigonometrical curve. When $\delta = 1$, the amplitude is larger for $\xi = 0$ (no-slip) and smaller for $\xi = 1$.The shear stress $\tau_{r\theta}$ increases at first monotonically up to a maximum which occurs at $\theta = \frac{\pi}{4}$ and $\theta = \frac{5\pi}{4}$ for $\xi = 0$. An opposite scenario occurs in the lower half when $\frac{\pi}{2} \leq \theta \leq \pi$ and $\frac{3\pi}{2} \leq \theta \leq 2\pi$. Here $\tau_{r\theta}$ decreases to a minimum value at $\theta = \frac{3\pi}{4}$ and $\theta = \frac{7\pi}{4}$ for $\xi = 0$ (see Figure 26(a)). From this we can conclude that the tangential stress is zero at the separation points $\theta = 0$

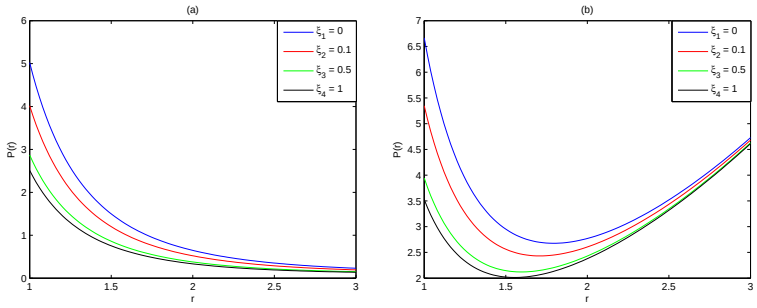

Figure 27: Variation of $p(r)$ with r where $\theta = 0^o$: (a) $\delta = 0.1$ (b) $\delta = 1$.

and $\theta = \pi$, positive at the top and negative at the bottom. A similar scenario is observed in higher values of δ. It can be noticed that the increase of both δ and ξ decreases the value of $\tau_{r\theta}$. Fixing ξ and varying δ displays a similar behavior, as demonstrated in Figure 26(b). When $\xi = 0$, $\tau_{r\theta}$ is larger for $\delta = 1$ and $\tau_{r\theta}$ is smaller for $\delta = 5$. It can be seen the amplitude increases/decreases as δ is lower/higher when ξ increases.

4.2.3 Pressure and vorticity for shear flow past a sphere

Pressure can be obtained from equation (26) or (27). The pressure equation is:

$$p(r,\theta) = p_0 - \mu\delta^2\Big(\frac{1}{2}r^2 + \frac{a^4}{3r^3}\beta\Big)\left(2\cos^2(\theta) - \sin^2(\theta)\right) \tag{52}$$

which after using (C-14) and (C-15) becomes

$$p(r,\theta) = p_0 - \mu\delta^2\Big(\frac{1}{2}r^2 + \frac{\lambda}{3r^3}\Big)\left(2\,\cos^2(\theta) - \sin^2(\theta)\right)$$

where p_0 is the integration constant.

The plots for the pressure and vorticity have the same behavior as in the uniform flow case (see **Section 4.1**). When $\delta = 0.1$, the pressure is a decreasing function of r. Further, pressure also decreases with increasing ξ (see Figure

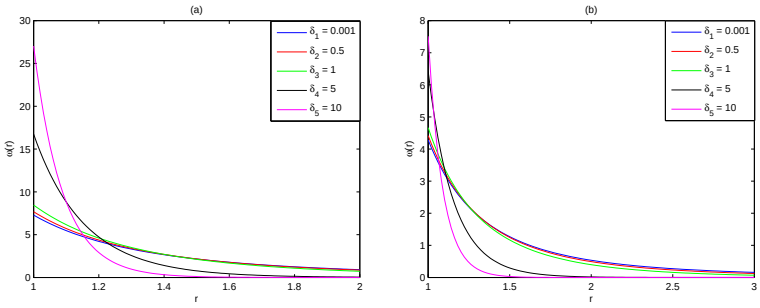

Figure 28: Variation of ω with r where $\theta = \frac{\pi}{4}$: (a) $\xi = 0.01$ (b) $\xi = 0.5$.

27(a)). For $\delta = 1$, the behavior is different in the sense that the pressure decreases for small r and then increases for greater r in all cases (see Figure 27(a)-(b)).

The vorticity ω is given by the expression:

$$\omega = \frac{a^{\frac{3}{2}}\gamma\delta}{2r^{\frac{1}{2}}} K_{\frac{5}{2}}(\delta\, r)\, \sin(\theta)\, \cos(\theta) \quad \hat{\mathbf{e}_\mathbf{z}} \tag{53}$$

also, we can rewrite it using (C-14) and (C-15) as

$$\omega = \frac{\eta\delta^4}{2}\, e^{\delta(a-r)} \left(\frac{1}{r} + \frac{3}{\delta\, r^2} + \frac{3}{\delta^2\, r^3}\right) \sin(\theta)\, \cos(\theta) \quad \hat{\mathbf{e}_\mathbf{z}}$$

The vorticity, while ξ fixed, decreases until it vanishes far away from the sphere surface $r \to \infty$. The rate of change of vorticity is very small when $\delta \ll 1$. The rate is increases when $\delta \approx 1$. However, forcing ξ to be fixed, we find the vorticity increases while we increase δ. In reverse, the vorticity decreases while we increase ξ (holding δ constant).

5 Force for the uniform flow past a cylinder/sphere

In this chapter we calculate the force acting on the cylinder/ sphere for the flows discussed in **chapter 3** and **4**. The force on the cylinder is calculated by integrating pressure and stress across the boundary as detailed in [16]. For the sake of brevity, we omit details and provide final expressions. In the case of uniform flow, the pressure contribution to the force is (calculated using (15)),

$$F_{\tau_{rr}} = -2\,\pi\,\mu\left(\delta^2\,a^2 + 2 + \frac{(a^2+2\,\xi)\,(a\,\delta\,K_1(\delta\,a) - 2\,K_0(\delta\,a))}{(a^2+2\,\xi)\,K_0(\delta\,a) + a\,\xi\,\delta\,K_1(\delta\,a)}\right)$$

and the shear stress contribution is (obtained using (14)),

$$F_{\tau_{r\theta}} = -2\,\pi\,\mu\left(\frac{(a^2+2\,\xi)\,(a\,\delta\,K_1(\delta\,a) + 2\,K_0(\delta\,a))}{(a^2+2\,\xi)\,K_0(\delta\,a) + a\,\xi\,\delta\,K_1(\delta\,a)} - 2\right)$$

Therefore, the total force on the cylinder embedded in Brinkman medium due to uniform flow is

$$\begin{aligned} F &= F_{\tau_{rr}} + F_{\tau_{r\theta}} \\ &= -2\,\pi\,\mu\,\delta^2\left[a^2 + \frac{2\,(a^2+2\,\xi)\,K_1(\delta\,a)}{\delta\left((a^2+2\,\xi)\,K_0(\delta\,a) + a\,\xi\,\delta\,K_1(\delta\,a)\right)}\right] \end{aligned} \tag{54}$$

Notice that the force depends on the key parameters δ (effective permeability) and ξ (slip coefficient) in addition to the radius a. When $\xi = 0$, the above (56) expression becomes

$$F = -2\,\pi\,\mu\,\delta^2\Big(a^2 + \frac{2\,K_1(\delta)}{\delta\,K_0(\delta)}\Big)$$

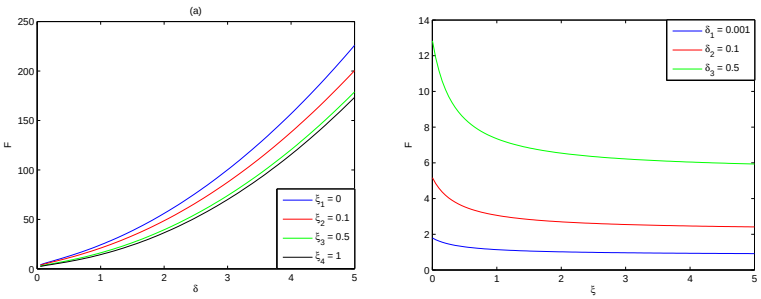

Figure 29: Variation of F for the uniform flow past a cylinder with: (a) δ for a fixed ξ (b) ξ for a fixed δ.

which corresponding to the force in the no-slip flow derived by [16]. In the limit $\xi \to \infty$ equation (56) yields

$$F = -2\,\pi\,\mu\,\delta^2 \left[a^2 + \frac{4\,K_1(\delta\,a)}{\delta\Big(2\,K_0(\delta\,a) + a\,\delta\,K_1(\delta\,a)\Big)} \right]$$

which the force acting on a pure-slip flow past a cylinder (a new result). The force given in (56) is plotted versus δ and ξ in Figure (29). As seen from the figure, the force increases with δ for each ξ. Also, the force is higher when $\xi = 0$, implying that the slip reduces the force, (Figure 29(a)). On the other hand, the force decreases with ξ, for fixed δ, and reaches a steady value. Also, F is greater for higher values of δ. We should remark that in the limit $\delta \to 0$, the force exhibits singular behavior (Stokes paradox).

The total force on a sphere in uniform flow is calculated using (42) and (41)

$$F = 2\,\pi\,\mu \left(\delta^2\,a^2 + \frac{3\,(a^3 + 2\,\xi)(\delta\,a + 1)}{a^3 + 3\,\xi + a\,\xi\,\delta} \right) \tag{55}$$

when $\xi = 0$, we obtain

$$F = 2\,\pi\,\mu\,(\delta^2\,a^2 + 3\,\delta + 3)$$

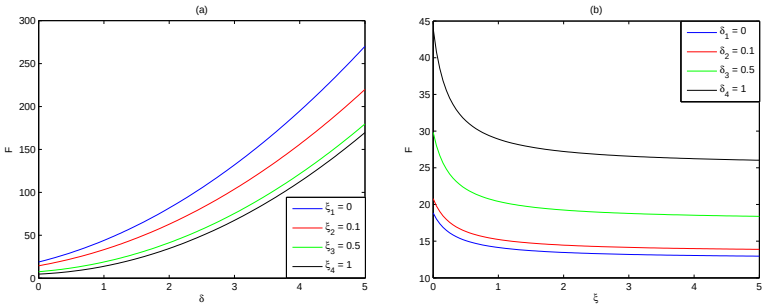

Figure 30: Variation of F for the uniform flow past a sphere with: (a) δ for a fixed ξ (b) ξ for a fixed δ.

which is the same as in [16] for no-slip flow. As $\xi \to \infty$, (57) gives

$$F = 2\,\pi\,\mu\left(\delta^2\,a^2 + 6 - \frac{12}{\delta\,a + 3}\right)$$

which expressed the force on a pure-slip flow past a sphere in a uniform flow. The plots for F with δ and ξ are shown in Figure 30(a)-(b). The behavior of force is qualitatively similar to that of the two-dimensional flow. However, the force exists for all values of δ and there is no singular behavior.

6 Conclusion

This thesis presented exact analytic solutions for the fourth order boundary-value problems arising in the study of porous media. The boundary-value problems discussed here model two and three-dimensional flows past a circular cylinder or sphere embedded in a Brinkman permeable medium. An important contribution here is the application of the Navier-slip boundary condition - not commanly utilised in the context of seepage flow - at the boundary of the cylinder/sphere. The second order vector differential equations for the velocity and pressure are transformed to the fourth order scalar differential equations via Stokes stream function formulation $\psi(r, \theta)$. The exact solutions determined are in closed form interms of modified Bessel functions, integral and fractional order of the first and second kinds. Our analytical results predicts the flow behavior, pressure, stresses and vorticity in the entire flow domain involving circular/spherical boundaries. It is shown that the physical quantities rely on two key parameters: (i) the effective permeability δ, and (ii) the slip coefficient ξ. Closed form expressions for the force acting on the cylinder/sphere are also calculated.

In two-dimensions, solutions are constructed for uniform flow and shear flow past a cylinder placed in a Brinkman medium (**Chapter 3**). The special cases of no-slip ($\xi = 0$) [13] [16] and pure-slip ($\xi \to \infty$) follow as special cases of our generalized results. An asymptotic analysis of the uniform flow past a cylinder reveals that when $\delta \to 0$ there is no solution to the boundary-value problem. This is the so called "Stokes paradox" observed in classical slow viscous flow [16]. Vorticity calculations show that there are two separation points in case of uniform flow while four separation points, one in each quadrant, exists for the extensional flow around a cylinder. The plots for the flow field, tangential velocity and stress, pressure and vorticity all indicate the significant

impact of the parameters δ and ξ.

Exact results for the uniform flow and extensional flow past a solid sphere are constructed in **Chapter 4**. Unlike flow in the two-dimensional case, the solution for the uniform flow past a sphere exists for all values of δ and consequently there is no paradox. When $\xi = 0$ our solution recovers the no-slip case [14] [16] and for $\xi \to \infty$ it gives the result for a perfect slip flow around a sphere. It is also demonstrated that the effective permeability and the coefficient of slip both influence the flow fields and relevant physical quantities.

The plots for the force indicate that the force is increasing function of δ for each ξ in two-dimensional case whereas it is an increasing function of the effective permeability for all slip. We expect that our predictions for the force, flow field behavior and physical quantities discussed above will provide valuable information in porous media application problems. Furthermore, our results can be used as a guide for possible generalizations of studies in seepage flow involving more general body profiles.

A summary of features of the flows based on our results

Uniform flow past a cylinder

- Flow is symmetrical with x and y axes.
- Two separation points in the flow and vorticity vanishes at these points.
- Streamlines get closer to the cylinder as δ and ξ increase.
- Velocity overshoot behavior, changes with δ and ξ.
- $\tau_{r\theta}$ is $2\,\pi$-periodic with varying amplitude due to ξ and δ.
- Lower pressure close to the cylinder and higher far away.
- Force is singular in the limit $\delta \to 0$ indicating the existence of the Stokes paradox.

Shear flow past a cylinder

- Flow is symmetrical with x and y axes.
- Four separation points in the flow one in each quadrant and vorticity vanishes at these points.
- Streamlines get closer to the cylinder as δ and ξ increase.
- Velocity overshoot behavior, changes with δ and ξ.
- $\tau_{r\theta}$ is π-periodic with varying amplitude due to ξ and δ.
- Force is zero.

Uniform flow past a sphere

- Two separation points on the symmetry axes.
- Qualitatively similar to two-dimensional flow.

- No paradox in three-dimensional flow.
- No singular behavior for the force in the limit $\delta \to 0$.

<u>Shear flow past a sphere</u>

- Streamlines changes infinitesimally while changing δ and ξ.
- Qualitatively similar to two-dimensional flow.
- No force.

Appendix A: Derivation of the general solution for two-dimensional flows

In this appendix we give a solution for (5), we use the separation of variables

$$\nabla^2\big(\nabla^2 - \frac{\mu^*}{\mu\, k}\big)\psi = 0, \tag{A-1}$$

Let:

$$\frac{\mu^*}{\mu\, k} = \delta^2, \tag{A-2}$$

$$\nabla^2\psi = \chi, \tag{A-3}$$

$$\big(\nabla^2 - \delta^2\big)\chi = 0 \tag{A-4}$$

First we begin solving (A-4) by searching for nonzero product solutions

$$\chi = R(r)\Theta(\theta) \qquad R,\Theta \neq 0,$$

here R is a function in r and Θ is a function in θ. Note since $\chi(r,\theta)$ necessarily 2π-periodic in θ then Θ is. (A-4) yields

$$\frac{r^2\, R''}{R} + \frac{r\, R'}{R} - \delta^2\, r^2 = -\frac{\Theta''}{\Theta} = \lambda \tag{A-5}$$

Here λ is the separation constant. Equivalently, we get

$$r^2\, R'' + r\, R' - \big(\delta^2\, r^2 + \lambda\big)\, R = 0, \tag{A-6a}$$

$$\Theta'' + \lambda\, \Theta = 0 \tag{A-6b}$$

Solving the Separated Equations (A-6) and (A-7). We first solve (A-8) under the stipulation of the periodic boundary condition $\Theta(2\pi) = \Theta(0)$. When $\lambda > 0$, the solution of Θ is

$$\Theta(\theta) = A\,\cos(\sqrt{\lambda}\,\theta) + B\,\sin(\sqrt{\lambda}\,\theta)$$

Where A,B are the integration constants. Using the periodic boundary condition implies that: if $\Theta \neq 0$, then we get $\sqrt{\lambda} = n \Rightarrow \lambda_n = n^2$, for all $n \in \mathbb{N}$. For each such $\lambda - value$, the nontrivial 2π-periodic solutions are constant multiples

$$\Theta_n(\theta) = A_n\,\cos(n\,\theta) + B_n\,\sin(n\,\theta) \tag{A-7}$$

where A_n, B_n are the integration constants. Next, we solve (A-6) when $\lambda = n^2$, for all $n \in \mathbb{N}$

$$r^2\,R'' + r\,R' - \left(\delta^2\,r^2 + n^2\right)R = 0$$

This is in fact modified Bessel equation. So the solution is

$$R_n(r) = C_n\,I_n(\delta\,r) + D_n\,K_n(\delta\,r) \tag{A-8}$$

Combining all the solutions yield the product solution for (A-4)

$$\begin{aligned}\chi(r,\theta) &= R(r)\,\Theta(\theta)\\ &= \sum_{n=0}^{\infty}\Big(C_n\,I_n(\delta\,r) + D_n\,K_n(\delta\,r)\Big)\Big(A_n\,\cos(n\,\theta) + B_n\,\sin(n\,\theta)\Big)\end{aligned} \tag{A-9}$$

Next we solve the equation (A-3). So we have two solutions the homogeneous solution and the particular solution. We start to find the homogeneous solution by solving

$$\nabla^2\psi = 0 \tag{A-10}$$

First we begin solving (A-11) by searching for nonzero product solutions

$$\psi = F(r)\Theta(\theta) \qquad F,\Theta \neq 0,$$

here F is a function in r and Θ is a function in θ. Note since $\psi(r,\theta)$ necessarily 2π-periodic in θ then Θ is. (A-11) yields

$$\frac{r^2\,F''}{F} + \frac{r\,F'}{F} = -\frac{\Theta''}{\Theta} = \lambda \tag{A-11}$$

Here λ is the separation constant. Equivalently, we get

$$r^2\,F'' + r\,F' - \lambda\,F = 0, \tag{A-12}$$

$$\Theta'' + \lambda\,\Theta = 0 \tag{A-13}$$

As before we solve the equation (A-14) to get the solution

$$\Theta_n(\theta) = A_n\,\cos(n\,\theta) + B_n\,\sin(n\,\theta) \tag{A-14}$$

where A_n, B_n are the integration constants. Next, we solve (A-13) when $\lambda = n^2$, for all $n \in \mathbb{N}$

$$r^2\,F'' + r\,F' - n^2\,F = 0 \tag{A-15}$$

This is in fact an Euler equation. The solution is

$$F_n(r) = \begin{cases} C_n\,r^n + D_n\,r^{-n} & \text{when} \quad \text{n} \geq 1 \\ C_0 + D_0\,\ln(r) & \text{when} \quad \text{n=0} \end{cases} \tag{A-16}$$

the general solution for equation (A-11) is

$$\psi_h(r,\theta) = C_0 + D_0\ \ln(r) + \sum_{n=1}^{\infty}\Big(C_n\, r^n + D_n\, r^{-n}\Big)\Big(A_n\ \cos(n\,\theta) + B_n\ \sin(n\,\theta)\Big) \tag{A-17}$$

Now, we find the particular solution for$\nabla^2\psi = \chi$. To find the particular solution, we use the variation of parameters method. We have two cases:

Case I: $n = 0$ The particular solution is

$$F_{p0}(r) = \frac{1}{\delta^2}\big(C_0\, I_0(\delta\, r) +, D_0\, K_0(\delta\, r)\big) = \text{constant} \tag{A-18}$$

Case II: $n \geq 1$

$$F_{pn}(r) = \frac{1}{\delta^2}\Big(C_n\, I_n(\delta\, r) - D_n\, K_n(\delta\, r)\Big) \tag{A-19}$$

Finally the particular solution for the equation (A-3) is

$$\psi_p(r,\theta) = \frac{1}{\delta^2}\sum_{n=1}^{\infty}\Big(C_n\, I_n(\delta\, r) - D_n\, K_n(\delta\, r)\Big)\Big(A_n\ \cos(n\,\theta) + B_n\ \sin(n\,\theta)\Big) \tag{A-20}$$

So, the general solution for equation (5) is:

$$\begin{aligned}\psi(r,\theta) = C_0 + D_0\ \ln(r) &+ \sum_{n=1}^{\infty}\Big(C_n\, r^n + D_n\, r^{-n}\Big)\Big(A_n\ \cos(n\,\theta) + B_n\ \sin(n\,\theta)\Big)\\ &+ \frac{1}{\delta^2}\sum_{n=1}^{\infty}\Big(E_n\, I_n(\delta\, r) - N_n\, K_n(\delta\, r)\Big)\Big(A_n\ \cos(n\,\theta) + B_n\ \sin(n\,\theta)\Big)\end{aligned} \tag{A-21}$$

Appendix B: Derivation of the general solution for three-dimensional flows

In this appendix we give a solution for (32), we use the separation of variables.

$$D^2\big(D^2 - \frac{\mu^*}{\mu\, k}\big)\psi = 0, \tag{B-1}$$

Let:

$$\frac{\mu^*}{\mu\, k} = \delta^2, \tag{B-2}$$

$$D^2\psi = \chi, \tag{B-3}$$

$$\big(D^2 - \delta^2\big)\chi = 0 \tag{B-4}$$

First we begin solving (B-4) by searching for nonzero product solutions:

$$\chi = R(r)\Theta(\theta) \qquad R,\Theta \neq 0,$$

here R is a function in r and Θ is a function in θ. Note since $\chi(r,\theta)$ necessarily 2π-periodic in θ then Θ is. (B-4) becomes

$$\frac{r^2\, R''}{R} - \delta^2\, r^2 = -\frac{\Theta''}{\Theta} + \cot\,\theta\,\frac{\Theta'}{\Theta} = n\big(n+1\big) \tag{B-5}$$

Here n is the separation constant. Equivalently, we get:

$$r^2\, R'' - \big(\delta^2\, r^2 + n\big(n+1\big)\big)\, R = 0, \tag{B-6}$$

$$\Theta'' - \cot\,\theta\,\Theta' + n\big(n+1\big)\,\Theta = 0 \tag{B-7}$$

Solving the Separated Equations (B-6) and (B-7). We first solve (B-7) using substitution method. Let: $x = \cos\,\theta$. (B-7) becomes

$$\frac{d}{dx}\left((1-x^2)\,\frac{d\Theta(x)}{dx}\right) + n\big(n+1\big)\,\Theta(x) = 0 \tag{B-8}$$

This is known as Legendre's differential equation where $\Theta(x) = P_n(x)$. $P_n(x)$ is one of the Legendre functions of the first order of order n and it is nite at $x = \pm 1$. There are also Legendre's functions of the second kind, $Q_n(x)$ but these are below up $x = \pm 1$ so They are not important in physics so we can ignore it. The solution for equation (B-7) is

$$\Theta(x) = P_n(x) \qquad \Rightarrow \qquad \Theta(\cos\,\theta) = P_n(\cos\,\theta) \tag{B-9}$$

Next, we solve (B-6) for all $n \in \mathbb{N}$. Equation (B-6) is in fact modified Bessel function of spherical coordinates of fractional order. The general solution is

$$R_n(r) = r^{\frac{1}{2}}\big(C_n\, I_{n+\frac{1}{2}}(\delta\, r) + D_n\, K_{n+\frac{1}{2}}(\delta\, r)\big) \tag{B-10}$$

Combining all the solutions yield the product solution for (B-4):

$$\begin{aligned}\chi(r,\theta) &= R(r)\,\Theta(\theta)\\ &= r^{\frac{1}{2}}\sum_{n=0}^{\infty}\left(C_n\, I_{n+\frac{1}{2}}(\delta\, r) + D_n\, K_{n+\frac{1}{2}}(\delta\, r)\right) P_n(\cos\,\theta)\end{aligned} \tag{B-11}$$

Back to solve the equation (B-3). So we have two solutions the homogeneous and particular solutions. Start by finding the homogeneous solution by solving:

$$D^2\psi = 0 \tag{B-12}$$

First we begin solving (B-12) by searching for nonzero product solutions:

$$\psi = H(r)\Theta(\theta) \qquad H,\Theta \neq 0,$$

here H is a function in r and Θ is a function in θ. Note since $\psi(r,\theta)$ necessarily 2π-periodic in θ then Θ is. That yields to

$$\frac{r^2\,H''}{H} = -\frac{\Theta''}{\Theta} + \cot\,\theta\,\frac{\Theta'}{\Theta} = n\big(n+1\big) \tag{B-13}$$

Here n is the separation constant. Equivalently, we get

$$r^2\,H'' - n\big(n+1\big)\,H = 0, \tag{B-14}$$

$$\Theta'' - \cot\,\theta\,\Theta' + n\big(n+1\big)\,\Theta = 0 \tag{B-15}$$

As before we solve the equation (B-15) to get the solution

$$\Theta(x) = P_n(x) \qquad \Rightarrow \qquad \Theta(\cos\,\theta) = P_n(\cos\,\theta) \tag{B-16}$$

Next, we solve (B-14) for all $n \in \mathbb{N}$. This is in fact an Euler equation. So the solution for (B-14) is

$$H_n(r) = A_n\,r^{-n} + B_n\,r^{n+1} \tag{B-17}$$

the general solution for equation (B-4) is

$$\psi_h(r,\theta) = \sum_{n=0}^{\infty}\Big(A_n\,r^{-n} + B_n\,r^{n+1}\Big)\,P_n(\cos\,\theta) \tag{B-18}$$

Now, we find the particular solution for:

$$D^2\psi = \chi \tag{B-19}$$

To find the particular solution, we use the variation of parameters method. We have two cases:

Case I: $n = 0$

$$H_{p0}(r) = \frac{r^{\frac{1}{2}}}{\delta^2}\left(C_0\, I_{\frac{1}{2}}(\delta\, r)+, D_0\, K_{\frac{1}{2}}(\delta\, r)\right) \tag{B-20}$$

Case II: $n \geq 1$

$$H_{pn}(r) = \frac{r^{\frac{1}{2}}}{\delta^2}\sum_{n=0}^{\infty}\left(C_n\, I_{n+\frac{1}{2}}(\delta\, r)+, D_n\, K_{n+\frac{1}{2}}(\delta\, r)\right) \tag{B-21}$$

Finally the particular solution for the equation (B-3) is

$$\psi_p(r,\theta) = \frac{r^{\frac{1}{2}}}{\delta^2}\sum_{n=0}^{\infty}\left(C_n\, I_{n+\frac{1}{2}}(\delta\, r) + D_n\, K_{n+\frac{1}{2}}(\delta\, r)\right) P_n(\cos\,\theta) \tag{B-22}$$

So, the general solution for equation (32) is:

$$\psi(r,\theta) = \sum_{n=0}^{\infty}\left(A_n\, r^{-n} + B_n\, r^{n+1} + \frac{r^{\frac{1}{2}}}{\delta^2}\left(C_n\, I_{n+\frac{1}{2}}(\delta\, r) + D_n\, K_{n+\frac{1}{2}}(\delta\, r)\right)\right) P_n(\cos\,\theta) \tag{B-23}$$

Appendix C: Some properties of the modified Bessel functions of second kind

All the identities that we used for modified Bessel function of the second kind of order ν ($\nu \in \mathbb{Z}$) [1]

$$K_{-\nu}(z) = K_\nu(z) \tag{C-1}$$

$$K_\nu(z) = K_{\nu+2}(z) - \frac{2(\nu+1)}{z} K_{\nu+1}(z) \tag{C-2}$$

$$K_\nu(z) = K_{\nu-2}(z) + \frac{2(\nu-1)}{z} K_{\nu-1}(z) \tag{C-3}$$

$$K_\nu(z) = \frac{z}{2\,\nu}\big(K_{\nu+1}(z) - K_{\nu-1}(z)\big) \tag{C-4}$$

The differentiation identities [1] have been used are

$$\frac{\partial}{\partial z} K_\nu(z) = -\frac{1}{2}\big(K_{\nu-1}(z) + K_{\nu+1}(z)\big) \tag{C-5}$$

$$\begin{aligned} \frac{\partial}{\partial z} K_\nu(z) &= -K_{\nu-1}(z) - \frac{\nu}{z} K_\nu(z) \\ &= \frac{\nu}{z} K_\nu(z) - K_{\nu+1}(z) \end{aligned} \tag{C-6}$$

$$\frac{\partial}{\partial z} K_0(z) = -K_1(z) \tag{C-7}$$

The integration identities have been used are

$$\int K_1(z)\, dz = -K_0(z) \tag{C-8}$$

$$\int z^{1-\nu}\, K_\nu(z)\, dz = -z^{1-\nu}\, K_{\nu-1}(z) \tag{C-9}$$

$$\int z^{\nu+1}\, K_\nu(z)\, dz = -z^{\nu+1}\, K_{-\nu-1}(z) \tag{C-10}$$

$$\int z\, K_1(z)\, dz = -z\, K_0(z) \tag{C-11}$$

All the identities that we used for modified Bessel function of the second kind of order $\nu + \frac{1}{2}$ ($\nu \in \mathbb{Z}$) [1]

$$K_{\nu+\frac{1}{2}}(z) = K_{-\nu-\frac{1}{2}}(z) \tag{C-12}$$

$$K_{\frac{1}{2}}(x) = \sqrt{\frac{\pi}{2\,x}}\, e^{-x} \tag{C-13}$$

$$K_{\frac{3}{2}}(x) = \sqrt{\frac{\pi}{2\,x}}\, e^{-x} \left(1 + x^{-1}\right) \tag{C-14}$$

$$K_{\frac{5}{2}}(x) = \sqrt{\frac{\pi}{2\,x}}\, e^{-x} \left(1 + 3x^{-1} + 3x^{-2}\right) \tag{C-15}$$

Here some elementary properties for differentiation the modified Bessel function of the second kind of fractional order [1]. Assuming $f_n(z) : (-1)^{n+1} \sqrt{\frac{\pi}{2\,z}}\, K_{n+\frac{1}{2}}(z)$ where $n \in \mathbb{Z}$

$$\frac{n+1}{z}\, f_n(z) + \frac{d}{dz}\, f_n(z) = f_{n-1}(z) \tag{C-16}$$

$$-\frac{n}{z}\, f_n(z) + \frac{d}{dz}\, f_n(z) = f_{n+1}(z) \tag{C-17}$$

References

[1] Abramowitz, M., Stegun, I. A., Handbook of Mathematical Functions with Formulas, Graphs, and Mathematical Tables, Dover, New York, 1964.

[2] Basset, A. B., A Treatise on Hydrodynamics, vol. 30, Ch. 21, 22, Cambridge, Deighton Bell, 1888.

[3] Brinkman, H. C., "A Calculation of The Viscous Force Exerted by a Flowing Fluid Dense Swarm of Particles," Applied Science Research, vol. 1, pp. 27-34, 1947.

[4] Brinkman, H. C., "On The Permeability of Media Consisting of Closely Packed Porous Particles," Applied Science Research, vol. 1, pp. 81-86, 1947.

[5] Darcy, H.R.P.G, Les Fontaines Publiques de la volle de Dijon, Vector Dalmont, Paris, 1856.

[6] Durlofsky, L., Brady, J.F., Analysis of the Brinkman equation as a model for flow in porous media, Phys. Fluids, vol.30, no,11, pp. 3329-3341, 1987.

[7] Happel, J., and Brenner, H., Low Reynolds Number Hydrodynamics, Prentice-Hall, Engelwood Cliffs, N.J.

[8] Khaled, A.-R.A, Vafai, K., "The Role of Porous Media in Modeling Flow and Heat Trnsfer in Biological Tissues," International Journal of Heat and Mass Transfer, vol. 46, pp. 4989-5003, doi:10.1016/S0017-9310(03)00301-6, 2003.

[9] Lauga, E., Brenner, M. P., and Stone, H. A., Microfluidics:The No-Slip Boundary Condition, in: C.Tropea et al.(eds.), Handbook of Experimental Fluid Mechanics,Springer, Berlin, p.1219, 2007.

[10] Lundgren, T.S., "Slow Flow Through Stationary Random Beds and Suspensions of Spheres," J. Fluid Mech., vol. 51, pp. 273-299, doi:10.1017/S002211207200120X, 1972.

[11] Nield, D. A., Bejan, A., Convection in Porous Media, Springer, New York, 2006.

[12] Palaniappan, D., "On Some General Solutions of Transient Stokes and Brinkman Equations," Journal of Theoretical and Applied Mechanics, vol. 52, no. 2, pp. 405-415, 2014.

[13] Pop, I., Cheng, P., "Flow Past A Circular Cylinder Embedded In A Porous Medium Based On The Brinkman Model," Int. J. Engng. Sci., vol. 30, no. 2, pp. 257-262, 1992.

[14] Pop, I., Ingham, D. B., "Flow Past A Sphere Embedded In A Porous Medium Based On The Brinkman Model," In. Comm. Heat Mass Transfer, vol. 23, no. 6, pp. 865-874, 1996.

[15] Tam, C.K. W., "The Drag on A Cloud of Spherical Particles in Low Reynolds number flow," J. Fluid. Mech., vol. 38, pp. 537-546, doi:10.1017/S0022112069000322, 1969.

[16] Wang, C. Y., "Darcy-Brinkman Flow with Solid Inclusions," Chem. Eng. Comm., vol. 197, pp. 261-274, 2010.

[17] Zhan, W., Xu, X. Y., "A Mathematical Model for Thermosensitive Liposomal Delivery of Doxorubicin to Solid Tumour," Journal of Drug Delivery, vol. 2013, Article ID 172529, 2013.